AUT Journal of Electrical Engineering
10.22060/EEJ.2026.25440.5933

Hybrid Fault-Tolerant Controller Based Nonlinear Model Predictive Control For a Flexible Satellite

Morteza Salehipour[1], Maryam Malekzadeh[2*], Mahdi Mortazavi[3]

[1]Mcs degree in Aerospace Engineering , Department of Aerospace Engineering , University of Isfahan ,Isfahan ,Iran

[2]Associate Professor , Department of Aerospace Engineering ,Sharif University of Technology, Tehran, Iran

[3]Associate Professor , Department of Aerospace Engineering ,University of Isfahan, Isfahan, Iran

Abstract:

This brief discusses the stabilization of a flexible satellite's attitude while considering actuator dynamics. It employs a constrained Lyapunov Nonlinear Model Predictive Control (LNMPC) method combined with the Feedback Linearization Technique (FBL). FBL is chosen for its ability to cancel the system's nonlinearity, making the control law easier to implement and more effective. more over the LNMPC is not able to nullify the low frequencies so it is necessary to combining it with a nonlinear controller. This composite controller aims for high accuracy in tracking the reference trajectory and, due to the LNMPC, provides tremendous robustness against unknown disturbances. The hybrid controller is designed to steer the satellite's attitude and bring the reaction wheel's angular momentum to zero to save energy. This paper addresses various challenges faced by satellites during their missions, including uncertainties, external torque disturbances, actuator faults, and vibrations of appendages. The performance of the proposed controller is analyzed while considering all these challenges. The active set method is used as the optimization algorithm, more over a nonlinear disturbance observer named Cascade Extended State Observer (Cascade ESO) is introduced to overcome the external disturbance and improve the performance of the controller and closed-loop stability is addressed using a candidate Lyapunov function.

Keywords:

Lyapunov nonlinear model predictive control , Feedback Linearization , flexible satellite , actuator fault, momentum management ,Cascade ESO, vibration suppression

2*Corresponding author's email: malekzadeh@sharif.edu

1.Introduction

By passing the time, space operations have gained tremendous attention from many outstanding researchers and scientists. satellites have evolved since 1957, when humans launched the first satellite into orbit. Nowadays, we witness the significant role that satellites play in various fields, such as military operations, telecommunications, and global internet access. Attitude control systems are important for any satellites, as they face numerous events during their missions that can disrupt their determined orientation. To address this issue, designing a robust controller can help overcome many challenges. So design a suitable satellite attitude control system is a significant factor and if the corresponding controller could not steer satellite to it's predetermined attitude, it leads to mission failed. In this paper, we utilize a nonlinear model predictive control method known as Lyapunov Nonlinear Model Predictive Control (LNMPC) to optimize the nonlinear dynamics and predict future behavior. This capability will enhance the robustness of the controller. By combining LNMPC with a nonlinear feedback linearization technique (FBL), we improve controller performance in the presence of uncertainty and mitigate the vibrations of flexible appendages, ensuring the satellite's attitude stability. This flexible satellite is equipped with three reaction wheels, and we have integrated the dynamics of these actuators into our algorithm. Several papers have been published by various researchers on this topic, and we have investigated some of them, NMPC is used in order to minimize the detumbling time of the satellite. In this algorithm a quadratic cost function is optimized by interior-point algorithm, moreover all the constraints and inherent under actuation is considered[1].Nonlinear Model Predictive Control(NMPC) is used for stabilizing a satellite that using magneto-torquers. This algorithm uses SQP to optimize the performance index[2]. In order to prevent detumbling phenomenon for a satellite with six magneto torquers, NMPC is utilized to guarantee satellite stability[3]. To tackle interplanetary rendezvous problem with low control authority, two NMPC algorithms are employed and each of them is responsible for interplanetary rendezvous with low thrust. This NMPC also uses SQP for optimizing [4].Manipulator mounted on a satellite is used for repairing or removing space debris from orbit. NMPC is used to guarantee realization of square reference end-effector trajectory[5]. In order to obstacle avoidance and trajectory planning of a free floating satellite manipulator, NMPC is employed to robust optimization and path following and real-time collision avoidance. This algorithm is used dynamics linearization to solve the problem[6]. NMPC is utilized to improve highly maneuver and capable of accurate trajectory tracking for a robot boat. This NMPC strategy has four control input with constraints, the cost function in this algorithm is solved by least square method based on trust region[7]. For stabilizing attitude of a marine satellite antenna, model predictive control is proposed to enhance the stabilization. This algorithm also implemented in Field Programmable Gate Array(FPGA), also it is needed to mention that This algorithm uses linear MPC[8]. In this paper PWA-MPC is utilized for a CubeSat attitude control, this CubeSat is equipped with solid thrusters so it can produce large eccentric torque, to tackle this issue MPC is employed to optimize and enhance the CubeSat performance [9]. Two NMPC algorithm are combined in order to active vibration suppression of a flexible satellite and attitude stabilization. Nonlinear auto regressive with exogenous inputs(NARX) neural network and nonlinear model predictive control (NMPC). NMPC in this algorithm uses sequential quadratic programming to optimizing the quadratic cost function[10]. Multi-horizon multi-model predictive control is designed in order to control an electromagnetic tethered satellite. The main benefit of this algorithm is having lower computational burden rather than classical MPC, also this algorithm uses NMPC to solve the problem[11].

Linear MPC and Feedback linearization are combined due to satellite attitude stabilization and steer angular velocity and attitude to zero, also this hybrid controller as tested on a satellite simulator[12]. Feedback linearization model predictive control is proposed for trajectory tracking of a quadcopter, feed back linearization is utilized to transform nonlinear dynamics to linear and linear MPC is designed to control the linearized system[13]. For a formation control of wheeled mobile robots(WMRs), linear model predictive control and input-output feed back linearization are employed to guarantee stability and robustness[14]. Nonlinear model predictive control and feedback linearization are combined for trajectory tracking and compliance constraints for an end-effector of an underactuated multibody system, MPC in this algorithm uses linear MPC [15]. Linear MPC combined with feedback linearization to optimize sequence of inputs over feedback linearized states and MPC predicts future states by leveraging a GPR model for a two-linked robot[16].Two novel double-loop fault-tolerant controllers to tackle the problems of stabilizing the attitude and nullifying appendage’s vibration of flexible satellite by integrating linear model predictive control(MPC) and sliding mode control(SMC)[17].Model Predictive Control(MPC) for Takagi-Sugeno fuzzy systems by combining the homogeneous polynomial technique and a switching mechanism is proposed, the switching model predictive control(SMPC) formulates a group of optimization problems to determine the control actions[18].Model Predictive Control for Nonlinear systems through quasi-Linear Parameter varying (qLPV) embedding is proposed. This algorithm uses three consecutive Quadratic programs (QPs) and a Moving -Horizon Estimation(MHE) scheme that predicts the behavior of the systems[19].Nonlinear model predictive Control is combined with Anti-Unwinding Sliding Mode Control(AUSMC) in order to nullify the low range frequency vibration of a flexible satellite[20].

We investigated the all the previous works related to NMPC and combining it with FBL. The LNMPC due to it’s different structure, because in this algorithm we formed a Toeplitz matrix with nonlinear dynamics and optimized it by active-set method so we develop a unique method in NMPC for flexible satellite attitude stabilization. The main contributions of this paper are categorized as follows:

1)Combining FBL with LNMPC in order to 3D kinematics and dynamics stabilizing and panels vibration neutralizing of a flexible satellite in the absence of damping with piezoelectric actuators on panels. Modified Rodriguez Parameters(MRPs) are considered as satellite kinematics.

2)Using active-set method as optimizer algorithm in order to optimize flexible satellite nonlinear dynamics, also we formed a Toeplitz matrix to involve nonlinear dynamics and candidate Lyapunov function into it.

3)Considering actuator dynamics in the algorithm and evaluating the system's performance in the presence of uncertainty, actuator faults and torque disturbance.

10.22060/EEJ.2026.25440.5933

4)Using Cascade ESO to reject disturbance and improve the performance of the hybrid controller

5)Hybrid controller is able to steer the reaction wheels angular momentum to zero after each maneuver to save more energy.

Section 2 provides an outline of the specific form of the appendages and piezo electrics and dynamics and kinematics of the flexible satellite, as well as the dynamics of reaction wheels. Section 3 separately focuses on control system design and actuator faults and Cascade ESO design, moreover a pseudocode of the active-set optimization is put at the end of this sections. Section 4 presents a rigorous stability analysis. Section 5 discusses simulation results under arbitrary conditions, and finally, Section 6 concludes the paper, highlighting the importance of our research

2-Mathematical model of the flexible satellite

This section outlines the dynamics and kinematics of the satellite in a detailed manner. It is divided into three subsections .Subsection 2-1 is discussed about the system description and assumptions, Subsection 2-2 focuses on the dynamics and kinematics of the satellite, while Subsection 2-3 discusses the dynamics of the reaction wheels.

2-1- System Description and Assumptions

Fig.1. illustrates the Flexible Satellite model[21]. The model consists flexible appendages which are attached to a rigid hub. The left and right panels are assumed as a beams connected to the rigid bulk body. furthermore , Piezoelectric layers are attached to each panel as patch.in this paper, the considered flexible satellite has 3 symmetrical solar panels attached to the center hub. More over, 3 reaction wheels are responsible for the attitude control of the satellite.

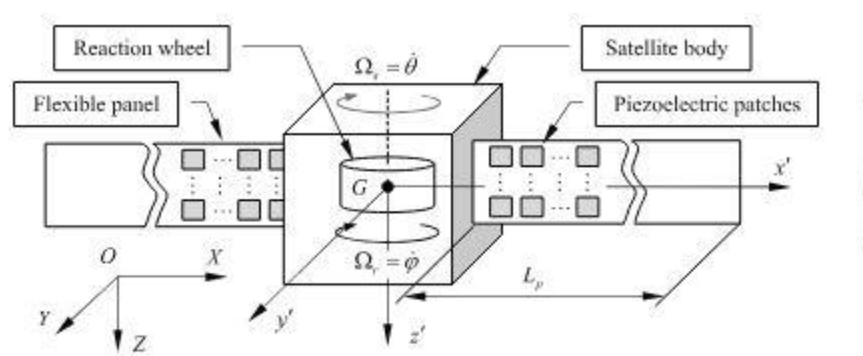

Fig.1.Flexible satellite components

10.22060/EEJ.2026.25440.5933

For better understanding, flexible satellite appendage's dynamics equations are derived[22]. The equations of motion are given by using Lagrange method

$$\frac{d}{dt}\left(\frac{\partial T}{\partial \psi}\right)-\frac{\partial T}{\partial \psi}+\frac{\partial U}{\partial \psi}=Q \tag{1}$$

Where $U=U_a+U_p$ and $T=T_a+T_p+T_h$ are strain energy and kinetic energy respectively. Q is the generalized force and a, p, h refer to the appendages, piezoelectric layers and central hub respectively. ψ is the satellite rotation angles and appendage's vibration coordinates. Eq. (2) is defined as position vector of an appendage element.

$$r_{a_i}=[x, y, z+w_i(w,t), 1]^T, i=1,2,... \tag{2}$$

Where $w_i(x,t)$ denotes the lateral deflection of the i th appendage. The velocity vector of an appendage element is given as follows

$$\dot{r}_R=\left(\sum_{j=1}^{3}\frac{\partial T_{a_i}^0}{\partial \theta_j}\dot{\theta}_j\right)r_{a_i}+T_{a_i}^0\dot{r}_{a_i}+v_0 \tag{3}$$

$$v_0=[-R_0\Omega, 0, 0, 0]^T \tag{4}$$

Where $T_{a_i}^0$ indicates the rotational/transitional matrix from the i th appendage frame to the orbital frame, R_0 is the distance from the satellite to the earth, Ω is the constant angular velocity of the satellite around the earth and $\theta_j (j=1,2,3)$ denotes the j th rotation angle of the satellite. The kinetic energy of the n th appendage is signified by the next equation

10.22060/EEJ.2026.25440.5933

$$T_{a_n}=\frac{1}{2}\int trace\{\dot{r}_R(\dot{r}_R)^T\}dm=\frac{1}{2}trace\{\sum_{j=1}^{3}\sum_{j=1}^{3}\frac{\partial T_{a_n}^0}{\partial\theta_j}\int r_{a_n}r_{a_n}{}^T dm(\frac{\partial T_{a_n}^0}{\partial\theta_i})^T\dot{\theta}_j\dot{\theta}_i\} \quad (5)$$

$$+$$

$$trace$$

$$\{\sum_{j=1}^{3}\frac{\partial T_{a_n}^0}{\partial\theta_j}\int r_{a_n}\dot{r}_{a_n}{}^T dm(T_{a_n}^0)^T\dot{\theta}_i\}+\frac{1}{2}trace\{T_{a_n}^0\int \dot{r}_{a_n}\dot{r}_{a_n}{}^T dm(T_{a_n}^0)^T\}+$$

$$trace\{\sum_{j=1}^{3}\frac{\partial T_{a_n}{}^0}{\partial\theta_j}\int r_{a_n}v_0{}^T dm\dot{\theta}_j\}+trace$$

$$\{T_{a_n}^0\int \dot{r}_{a_n}v_0{}^T dm\}+$$

$$\frac{1}{2}trace\{\int v_0v_0^T dm\}$$

Eq. (6) is the kinetic energy of the piezoelectric layers on the k th appendage.

$$T_{p_{a_k}}=\frac{1}{2}\sum_{n=1}^{N_k}\int trace\{\dot{r}_R(\dot{r}_R)^T\}dm \quad (6)$$

$$=\frac{1}{2}\sum_{n=1}^{N_k}trace\{\sum_{j=1}^{3}\sum_{j=1}^{3}\frac{\partial T_{a_n}^0}{\partial\theta_j}\int r_{a_n}r_{a_n}{}^T dm(\frac{\partial T_{a_n}^0}{\partial\theta_i})^T\dot{\theta}_j\dot{\theta}_i\}$$

$$+\sum_{n=1}^{N_K}trace\{\sum_{i=1}^{3}\frac{\partial T_{a_n}^0}{\partial\theta_i}\int r_{a_n}\dot{r}_{a_n}{}^T dm(T_{a_n}^0)^T\dot{\theta}_i\}$$

$$+\frac{1}{2}\sum_{n=1}^{N_k}trace\{T_{a_n}^0\int \dot{r}_{a_n}\dot{r}_{a_n}{}^T dm(T_{a_n}^0)^T\}$$

$$+\sum_{n=1}^{N_k}trace\{\sum_{j=1}^{3}\frac{\partial T_{a_n}^0}{\partial\theta_j}\int r_{a_n}v_0^T dm\dot{\theta}_j+T_{a_n}^0\int \dot{r}_{a_n}v_0^T dm\}$$

$$+\frac{1}{2}\sum_{n=1}^{N_k}trace\{\int v_0v_0^T dm\}$$

Where N_k is the number of the piezoelectric layers on the k th appendage.

10.22060/EEJ.2026.25440.5933

$$T_h = \frac{1}{2}\int trace\{\dot{r}_R(\dot{r}_R)^T\}dm$$
$$= \frac{1}{2}trace\{\sum_{j=1}^{3}\sum_{j=1}^{3}\frac{\partial T_h^0}{\partial\theta_j}\int r_h r_h^T dm(\frac{\partial T_h^0}{\partial\theta_i})^T\dot{\theta}_j\dot{\theta}_i\}$$
$$+trace\{\sum_{j=1}^{3}\frac{\partial T_h^0}{\partial\theta_j}\int r_h v_0^T dm\dot{\theta}_j\}+\frac{1}{2}trace\{\int v_0 v_0^T dm\} \quad (7)$$

The potential energy of the appendages are given by the following equations

$$U_a = \frac{1}{2}\sum_{i=1}^{2} Ez^2(\frac{\partial^2 w_i}{\partial x^2})^2 dv \quad (8)$$

$$U_p = \frac{1}{2}\sum_{n=1}^{N}\int E_p z^2(\frac{\partial^2 w_{p_n}}{\partial x^2})^2 dv + \sum_{n=1}^{N} ze_{31}E_{z_n}\frac{\partial^2 w_{p_n}}{\partial x^2}dv$$
$$+\frac{1}{2}\sum_{n=1}^{N} E_{z_n} d_n dv \quad (9)$$

Where d_n is the electric displacement for the nth patch and it is given as follows

$$d_n = \varepsilon_{p_n}\frac{v_n}{h_{p_n}} \quad (10)$$

The Eq. (11) indicates the electric field in the nth piezoelectric layer.

$$E_{z_n} = \frac{v_n}{h_{p_n}} \quad (11)$$

ε_{p_n} indicates the dielectric constant of the piezoelectric material that forms the nth patch.

2-2-Dynamics and Kinematics Equations

In this subsection, the nonlinear dynamics and kinematics related to the flexible satellite are defined[17],[23]. Eqs. (12) and (13) represent the nonlinear dynamics of the flexible satellite. The flexible

10.22060/EEJ.2026.25440.5933

satellite's structure is characterized by its moment of inertia $\boldsymbol{I}_s \in \boldsymbol{R}^3$ and $\boldsymbol{\omega} \in \boldsymbol{R}^3$ is the flexible satellite angular velocities , $\boldsymbol{\delta}_n \in \boldsymbol{R}^{3\times n}$ denotes the coupling matrix between rigid and flexible parts of the satellite , $\boldsymbol{\eta}_n \in \boldsymbol{R}^{3\times n}$ is flexible appendage's vibration displacements , $\boldsymbol{u} \in \boldsymbol{R}^3$ and $\boldsymbol{d} \in \boldsymbol{R}^3$ are control inputs and external disturbances respectively . $\boldsymbol{C} = 2\xi\boldsymbol{\Omega}_f \in \boldsymbol{R}^{n\times n}$ and $\boldsymbol{K} = \boldsymbol{\Omega}^2{}_f$ are damping matrix and stiffness coefficients respectively. $\boldsymbol{\delta}_p \in \boldsymbol{R}^{3\times p}$ and $\boldsymbol{u}_p \in \boldsymbol{R}^3$ are the coupling matrix related to the flexible appendage and piezoelectric voltage control input respectively.

$$\boldsymbol{I}_s\dot{\boldsymbol{\omega}} + \boldsymbol{\delta}'\ddot{\boldsymbol{\eta}} + \boldsymbol{\omega}^{\times}(\boldsymbol{I}_s\boldsymbol{\omega} + \boldsymbol{\delta}'\dot{\boldsymbol{\eta}}) - \boldsymbol{\omega}^{\times}\boldsymbol{h}_{\omega} = \boldsymbol{u} + \boldsymbol{d}_{disturbance} \quad \textbf{(12)}$$

$$\ddot{\boldsymbol{\eta}} + \boldsymbol{C}\dot{\boldsymbol{\eta}} + \boldsymbol{K}\boldsymbol{\eta} + \boldsymbol{\delta}\dot{\boldsymbol{\omega}} = -\boldsymbol{\delta}_p\boldsymbol{u}_p \quad \textbf{(13)}$$

$$\boldsymbol{h}_{\omega} = \boldsymbol{I}_{\omega}\boldsymbol{\omega} \quad \textbf{(14)}$$

Eqs. (15) and (16) are related to the Modified Rodriguez Parameters(MRPs) , and is the identity matrix and the notation is the skew symmetric matrix[23].

$$\dot{\boldsymbol{\sigma}} = \boldsymbol{G}(\boldsymbol{\sigma})\boldsymbol{\omega} \quad \textbf{(15)}$$

$$\boldsymbol{G}(\boldsymbol{\sigma}) = \frac{1}{4}((1-\boldsymbol{\sigma}'\boldsymbol{\sigma})\boldsymbol{I}_3 + 2\boldsymbol{\sigma}^{\times} + 2\boldsymbol{\sigma}\boldsymbol{\sigma}' \quad \textbf{(16)}$$

Eq. (17) is about the complexity of the model so we need to separate the momentum of inertia of the flexible satellite from the coupling matrix. In this research the Eq. (17) is substituted to Eq. (12).

$$\boldsymbol{I}_{sp} = \boldsymbol{I}_s - \boldsymbol{\delta}'\boldsymbol{\delta} \quad \textbf{(17)}$$

Eqs. (18) and (19) are discussed about the piezoelectric actuators that attached on the solar panels as patches.[24]

$$\boldsymbol{y}_p = \boldsymbol{P}\dot{\boldsymbol{\eta}} \quad \textbf{(18)}$$

10.22060/EEJ.2026.25440.5933

$$u_p = \delta^{'} y_p \tag{19}$$

2-3-Actuators Dynamics Equations

In this subsection, we define the dynamics of the actuator[25]. Reaction wheels are typically DC motors mounted within a satellite, allowing them to rotate in any direction along the axis frame. Eq. (20) represents the differential equation governing the armature of the DC motor circuits R_α. L_α is the armature inductance, K_b is a constant related to the back electromotive force (emf), Ω is the angular velocity of the reaction wheel motor, i_α is the armature current and e_α is the applied armature voltage.

$$L_\alpha \frac{di_\alpha}{dt} + R_\alpha i_\alpha + K_b \Omega_{(i)} = e_\alpha, i = 1,2,3 \tag{20}$$

In Eq. (21), θ is the angular displacement of the motor shaft.

$$e_\alpha = K_b \frac{d\theta}{dt} \tag{21}$$

Eq. (22) is the proportional of the torque which is produced by the motors to the armature current.

$$u_r(i) = K_m i_\alpha \tag{22}$$

The remaining equations relate to the angular velocity of the reaction wheels. By substituting Eqs. (23), (24), and (25) into Eq. (12), the influence of actuator dynamics on satellite dynamics will be incorporated.

$$\dot{\Omega}_{(i)} + \frac{1}{T_m}\Omega_{(i)} = \frac{K_t}{T_m} e_\alpha \tag{23}$$

AUT Journal of Electrical Engineering
10.22060/EEJ.2026.25440.5933

$$I_{\omega}(i)\dot{\Omega}_{(i)}+\frac{I_{\omega}(i)}{T_m}\Omega_{(i)}=I_{\omega}(i)\frac{K_t}{T_m}e_{\alpha} \tag{24}$$

$$I_{\omega}(\dot{\omega}+\dot{\Omega})=I_{\omega}K_tT_m{}^{-1}e_{\alpha}-I_{\omega}T_m{}^{-1}(\omega+\Omega)=u_r \tag{25}$$

$$(I_s-I_{\omega})(\dot{\omega})=-\omega^{\times}(I_s\omega+I_{\omega}\Omega)-(I_{\omega}K_tT_m{}^{-1}(\omega+\Omega))+T_d \tag{26}$$

3-Satellite Attitude Controller Design

In this section, the proposed hybrid controller is defined. The LNMPC and FBL are outlined separately. Fig.2 depicts the entire structure of the hybrid controller. The output of the LNMPC is entering to the system and FBL also is entering for canceling the nonlinearity of the LNMPC output then employ the produced control law to the flexible satellite dynamic in the presence of actuators fault and external torque disturbance. It aims to steer predicted output $\tilde{y}$ to the reference trajectory y furthermore this combination helps to simplify the control law and reduce computation burden by canceling the nonlinearities.

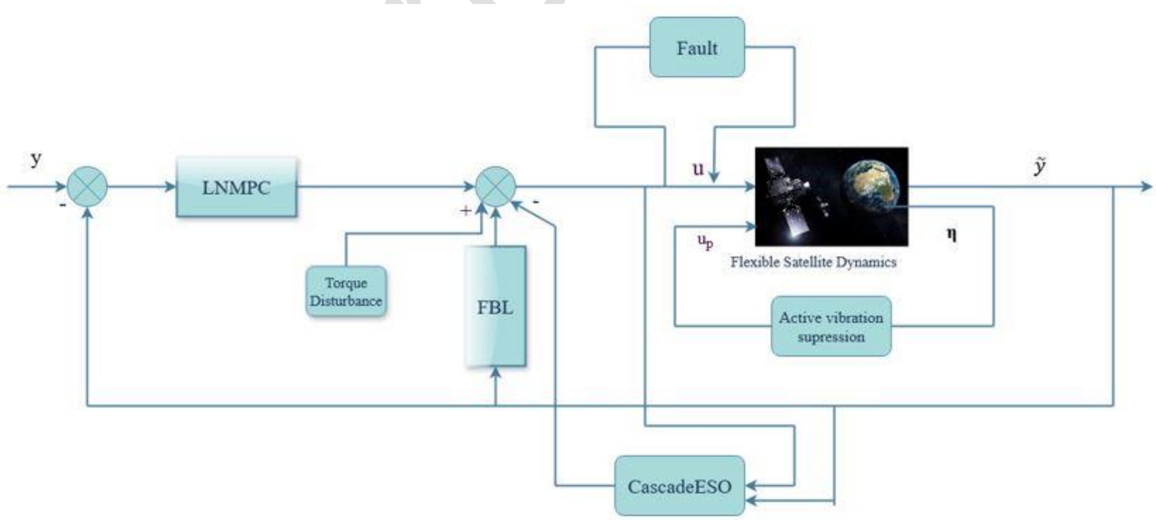

Fig.2.Structure of the hybrid controller

10.22060/EEJ.2026.25440.5933

3-1- Reaction Wheels Faults

Actuator faults means, actuators performance degradation. According to[25] the fault entering to actuators equation is given,

$$u = Eu_c + \bar{u} \tag{27}$$

Where $E = diag(e_1, e_2, e_3 ..., e_n)$ with $0 \le e_i \le 1 (i = 1, 2, ..., n)$ is the effectiveness of the actuators, $u_c = \begin{bmatrix} u_{c,1} & u_{c,2} & \cdots & u_{c,n} \end{bmatrix}^T$ is the command inputs of the reaction wheels.

3-2-Nonlinear Model Predictive Control Approach

This section describes the procedure for Lyapunov nonlinear model predictive control, which aims to stabilize satellite attitude. The[26] Lyapunov nonlinear model predictive control algorithm utilizes nonlinear dynamics organized within a Toeplitz matrix, incorporating a candidate Lyapunov function into the matrix. Eq. (28) presents this candidate Lyapunov function V , which estimates both the reference trajectory and predicted model of the system and it is indicated by and respectively. Furthermore, the P matrix is a positive symmetric matrix and it is discussed in section 4.

$$V = e^{'} Pe \tag{28}$$

$$e = \tilde{y} - y \tag{29}$$

$$J_{\cos t} = \min \left\{ \sum_{j=N}^{N_p} Q_j (\tilde{y}(k+j \mid k) - y(k+j \mid k))^2 + \sum_{i=0}^{N_u - 1} R_i (\Delta u(k+i \mid k)) \right\} \tag{30}$$

Eq. (30) represents the desired cost function, which aims to optimize system behavior within a finite time horizon. The parameters are denoted as weighting matrices used to track errors in the prediction horizon. The weighting matrix is utilized to increase the control input within the control horizon. In vector form, the system prediction is computed as follows: Eq.(30) is signifies the aimed equation that is indicated a vector of the predicted output of the system in a finite time prediction horizon $(N_1, N_2, N_3, ...N_p)$ Parameters Q denotes the weighting matrix to tracking the error in a prediction horizon. R is the weighting matrix in order to increment control input in a control horizon N_u . In a vectorial form the system prediction is computed by

10.22060/EEJ.2026.25440.5933

$$\tilde{\boldsymbol{Y}} = \boldsymbol{F} + \boldsymbol{G}\Delta\boldsymbol{u} \tag{31}$$

$$\tilde{\boldsymbol{Y}} = \begin{bmatrix} \tilde{y}(\boldsymbol{k}+1|\boldsymbol{k}) \\ \tilde{y}(\boldsymbol{k}+2|\boldsymbol{k}) \\ \vdots \\ \tilde{y}(\boldsymbol{k}+\boldsymbol{N}_p|\boldsymbol{k}) \end{bmatrix} \tag{32}$$

$$\Delta\boldsymbol{u} = \begin{bmatrix} \Delta\boldsymbol{u}(\boldsymbol{k}|\boldsymbol{k}) \\ \Delta\boldsymbol{u}(\boldsymbol{k}+1|\boldsymbol{k}) \\ \vdots \\ \Delta\boldsymbol{u}(\boldsymbol{k}+\boldsymbol{N}_u-1|\boldsymbol{k}) \end{bmatrix} \tag{33}$$

Eq.(31) is presented the predicted model of the nonlinear dynamic of the flexible satellite, the corresponding outputs are kinematics and dynamics of the system and Eq.(32) is denoted the predicted model vector and is the one step of the predicted model so it continues over the $\boldsymbol{N}_p$ so $\boldsymbol{F}$ and $\boldsymbol{G}$ are considered as free response with dimension $\boldsymbol{N}_p \times 1$ and force response with dimension $\boldsymbol{N}_p \times \boldsymbol{N}_u$ respectively and they are given by the following equations, $\boldsymbol{y} = [\boldsymbol{\sigma}, \boldsymbol{\omega}, \boldsymbol{h}_\omega]$ are the steady states of the system and $\Delta\boldsymbol{u}$ is the control effort variation vector. Eq.(34) is a Toeplitz matrix that is formed by the future estimated behavior of the system over a finite prediction horizon $\boldsymbol{N}_p$ In this research it is assumed that, prediction horizon and control horizon $\boldsymbol{N}_u$ are the same.

10.22060/EEJ.2026.25440.5933

$$G=\begin{bmatrix} \dfrac{\partial\tilde{y}(k+1)}{\partial\Delta u(k)} & 0 & \cdots & 0 \\ \dfrac{\partial\tilde{y}(k+2)}{\partial\Delta u(k)} & \dfrac{\partial\tilde{y}(k+2)}{\partial\Delta u(k+1)} & \cdots & 0 \\ \vdots & \vdots & \ddots & \vdots \\ \dfrac{\partial\tilde{y}(k+N_p)}{\partial\Delta u} & \dfrac{\partial\tilde{y}(k+N_p)}{\partial\Delta u(k+1)} & \cdots & \dfrac{\partial\tilde{y}(k+N_p)}{\partial\Delta(k+N_u-1)} \end{bmatrix} \tag{34}$$

$$F=\begin{bmatrix} \tilde{y}_1 \\ \tilde{y}_2 \\ \vdots \\ \tilde{y}_{N_p} \end{bmatrix} \tag{35}$$

Eq.(36) is the modified form of the quadratic cost function that is used to solve the optimization problem. and will be obtained by solving the Eqs. (37) and (38).

$$J_{\cos t}=\frac{1}{2}\Delta u^2\phi\Delta u+\theta^T\Delta u \tag{36}$$

$$\phi=2(G^TQG+R) \tag{37}$$

$$\theta=G^TQ(F-Y) \tag{38}$$

Parameters Q and R are the diagonal weighting matrices that related to set point tracking and control effort respectively. In this research the active-set method is utilized due to solving the optimization. Active-set method for the aim of it's speed and accuracy it is superior to SQP.

10.22060/EEJ.2026.25440.5933

3-3- Constraints mapping

One of the advantages of the NMPC is taking constraints into account, so the control effort and control effort variation limitation are given below and it is restricted over the prediction horizon.

$$\boldsymbol{u}_{\min} \le \boldsymbol{u}(\boldsymbol{k}+\boldsymbol{i} \mid \boldsymbol{k}) \le \boldsymbol{u}_{\max} \tag{39}$$

$$\Delta\boldsymbol{u}_{\min} \le \Delta\boldsymbol{u}(\boldsymbol{k}+\boldsymbol{i} \mid \boldsymbol{k}) \le \Delta\boldsymbol{u}_{\max} \tag{40}$$

3-4- Feedback Linearication Technique

this subsection is devoted to the feedback linearization teqchnique. Generally solving the equations are inspired by [27] and [28]. Eqs.(41) and (42) are defined the nonlinear equations of the purposed satellite once again.

$$\dot{\boldsymbol{X}} = \boldsymbol{f}(x) + \boldsymbol{g}(x)\boldsymbol{u} \tag{41}$$

$$\boldsymbol{f}(x) = \begin{bmatrix} \boldsymbol{G}(\boldsymbol{\sigma})\boldsymbol{\omega} \\ \boldsymbol{I}_s^{-1}(-\boldsymbol{\omega}^{\times}\boldsymbol{I}_s\boldsymbol{\omega} + \boldsymbol{\delta}'\dot{\boldsymbol{\eta}}) - \boldsymbol{\delta}^T\ddot{\boldsymbol{\eta}} + \boldsymbol{u} + \boldsymbol{d} \\ 0 \end{bmatrix} \tag{42}$$

$$\boldsymbol{g}(x) = \begin{bmatrix} 0_3 \\ \boldsymbol{I}_s^{-1} \\ -\boldsymbol{I}_3 \end{bmatrix} \tag{43}$$

In Eq.(44) the output equation of the system is given, we need to obtain a linear relation between input and output of the system.

$$\tilde{y} = \boldsymbol{h}(x) = \tilde{\sigma} + \alpha\tilde{\boldsymbol{h}}_{\omega} \tag{44}$$

10.22060/EEJ.2026.25440.5933

$$\begin{bmatrix} \tilde{y}_1^{(r_1)} \\ \tilde{y}_2^{(r_2)} \\ \tilde{y}_3^{(r_3)} \end{bmatrix} = \boldsymbol{E}(\boldsymbol{x}) + \boldsymbol{D}(\boldsymbol{x})\boldsymbol{u} \tag{45}$$

Where $\boldsymbol{E}(\boldsymbol{x})$ and $\boldsymbol{D}(\boldsymbol{x})$ are given as follows

$$\boldsymbol{E}(\boldsymbol{x}) = \begin{bmatrix} L_f^{r_1} h_1(x) \\ L_f^{r_2} h_2(x) \\ L_f^{r_3} h_3(x) \end{bmatrix} \tag{46}$$

$$\boldsymbol{D}(\boldsymbol{x}) = \begin{bmatrix} L_{g_1} L_f^{r_1-1} h_1(x) & \cdots & L_{g_3} L_f^{r_3-1} h_1(x) \\ \vdots & \ddots & \vdots \\ L_{g_1} L_f^{r_3-1} h_1(x) & \cdots & L_{g_3} L_f^{r_3-1} h_1(x) \end{bmatrix} \tag{47}$$

If $\det(\boldsymbol{D}(\boldsymbol{x})) \neq 0$ this means $\boldsymbol{D}(\boldsymbol{x})$ is not singular and feedback linearization is possible.Next step, it is needed to taking time derivative until a relation between input and output achieves.

$$\dot{y} = \frac{\partial h(x)}{\partial x}\dot{x} = \frac{\partial h(x)}{\partial x}(f(x) + g(x)u) = L_f h(x) + L_g h(x)u \tag{48}$$

Eq.(48) is the first time derivative of the system output where $L_f h(x)$ is called Lie derivative of $h(x)$ respect to f .By taking the second time derivative the input is appeared so we realized that the degree of the system is $r_1 = 2$. Eq.(49) is denoted the second time derivative.

$$\ddot{\tilde{y}} = \ddot{\tilde{\sigma}} + \alpha \ddot{\tilde{h}}_\omega \tag{49}$$

10.22060/EEJ.2026.25440.5933

$$\tilde{\ddot{y}} = \frac{\partial^2 \boldsymbol{h}}{\partial^2 \boldsymbol{x}} \dot{\boldsymbol{x}} = \boldsymbol{L}_f^{\ 2} \boldsymbol{h}(\boldsymbol{x}) + \boldsymbol{L}_g \boldsymbol{L}_f \boldsymbol{h}(\boldsymbol{x}) \boldsymbol{u} \tag{50}$$

Assume $\tilde{\ddot{\boldsymbol{y}}} = \boldsymbol{v}$ so the virtual input is designed and by substituting it into the Eq.(45) is obtained.

$$\boldsymbol{v} = \boldsymbol{E}(\boldsymbol{x}) + \boldsymbol{D}(\boldsymbol{x})\boldsymbol{u} \tag{51}$$

$$\boldsymbol{u} = \boldsymbol{D}(\boldsymbol{x})^{-1}(\boldsymbol{v} - \boldsymbol{E}(\boldsymbol{x})) \tag{52}$$

Where

$$\boldsymbol{v} = -\boldsymbol{K}_e \boldsymbol{e} - \boldsymbol{K}_e \dot{\boldsymbol{e}} \tag{53}$$

Eq. (53) denotes the virtual input and $\boldsymbol{e} = \tilde{\boldsymbol{y}} - \boldsymbol{y}$ is the difference between future and past behavior of the system $\boldsymbol{K}_e$ and are the weighting matrices.

3-5-pseudocode for the combined algorithms

In this subsection a simple pseudocode to enhance the reproducibility of the hybrid scheme is outlined. at first, for the Lyapunov Nonlinear Model Predictive Control a quadratic objective function is put[29].

$$\boldsymbol{J} = \frac{1}{2} \Delta \boldsymbol{u}^T \Phi \Delta \boldsymbol{u} + \boldsymbol{\theta}^T \Delta \boldsymbol{u} \tag{54}$$

s.t

$$\boldsymbol{A} \Delta \boldsymbol{u} \leq \boldsymbol{b} \tag{55}$$

This algorithm is prepared due to clarify the active-set method. In addition, the optimized control effort which is gained by this algorithm is used in all the hybrid algorithm and all the variables are introduced in the section 3.

Algorithm 1: optimizing LNMPC using Active-set
Input: $\Phi, \boldsymbol{\theta}, \boldsymbol{A}, \boldsymbol{b}$
$\boldsymbol{u}_0$ (first element of the optimized step)

10.22060/EEJ.2026.25440.5933

$\varepsilon \succ 0$ (optimization tolerance)

Output : u^* (optimized control input)

1. **Initializing**

   $u \leftarrow u_0$

   Determining a set for equality constraints w_{set} for each step

   $\{\min \|A\Delta u - b\| \leq \varepsilon\} \rightarrow w_{set}$

   To minimize the objective function subject to the equality constraints, lagrange multipliers are utulized.

   $\lambda = -(A \times \Phi^{-1} \times A^T)^{-1}(b + A \times \Phi^{-1} \times \theta)$

2. Creating a loop and analyze the active constraints for each step

   For $k = 0,1,2,3,....,N_p - 1$

   If $\lambda \geq 0$

   u^* is calculated

   Else if $\lambda \prec 0$

   It is necessary to Remove the negative elements of the constraints set to avoid inactivity

   $w_{set} \leftarrow w_{set} \setminus \lambda\_negative$ or $w_{set}.remove(\lambda\_negative)$

   Next step we need to upgrade the optimized answer by a time step named α

   $u^* = u^* + \alpha u^*$

   At the end the control effort derivative is determined as follows

   $\Delta u(k) = u^*(k) - u^*(k-1)$

   End Loop

The optimized control effort which is achived by the above algorithm will combine into the FBL which is discussed in the section 3-4 and then hybrid optimzed control effort derivative is implied to the flexible satellite nonlinear dynamics.

3-6-Cascade ESO Design

In this subsection, the procedure of Cascade ESO is outlined[30]. Two layers are designed and the Eqs.(56) and (57) are represented their mathematical formulas rigorously. In Eq.(42) the first layer is designed and in Eq.(56) the second layer is designed. and are the estimated of the steady states related to the first and second layer respectively.

10.22060/EEJ.2026.25440.5933

$$\begin{cases} e_1(t) = z_1(t) - \tilde{y}(t) \\ \dot{z}_1 = z_2 - \beta_1 e_1(t) + \bar{b}_0 u(t) \\ \dot{z}_2(t) = -\beta_2\, fal(e_1(t), \alpha_1, \delta_1) \end{cases} \tag{56}$$

$$\begin{cases} e_{s_1}(t) = s_1(t) - \tilde{y}(t) \\ \dot{s}_1(t) = s_2(t) - \beta_3 e_{s_1}(t) + z_2(t) + \bar{b}_0\, u(t) \\ \dot{s}_2(t) = -\beta_4\, fal(e_{s_1}(t), \alpha_2, \delta_2) \end{cases} \tag{57}$$

Eq.(58) is a continuous function that is used in the designed equations.

$$fal(e, \alpha, \delta) = \begin{cases} \dfrac{e}{\delta^{1-\alpha}}, |e| \prec \delta \\ |e|^{\alpha}\, sign(e), |e| \geq \delta \end{cases} \tag{58}$$

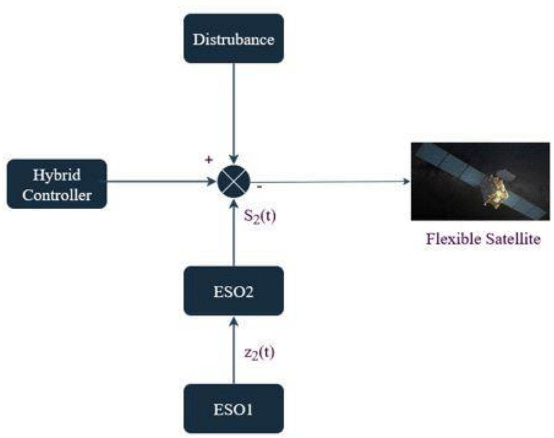

Fig.3.Structure of the Cascade ESO

4-Stability analysis

This section is inspired by [12], and Eq. (59) is outlined the linearized model of the output. The output is about steering kinematics and reaction wheels momentum wheels to zero.

10.22060/EEJ.2026.25440.5933

$$\begin{Bmatrix} z_1 = h_1(x) = \sigma_1 + \alpha h_1 \omega \\ z_2 = h_2(x) = \sigma_2 + \alpha h_2 \omega \\ z_3 = h_3(x) = \sigma_3 + \alpha h_3 \omega \end{Bmatrix} \tag{59}$$

$$\begin{Bmatrix} z_4 = L_f h_1(x) = \dot{\sigma}_4 + \alpha \dot{h}_4(x) \\ z_5 = L_f h_2(x) = \dot{\sigma}_5 + \alpha \dot{h}_5(x) \\ z_6 = L_f h_3(x) = \dot{\sigma}_6 + \alpha \dot{h}_6(x) \end{Bmatrix} \tag{60}$$

Eq. (60) is denoted the output error and the predicted output arrives at the reference trajectory or and it is set to be zero.

$$\begin{Bmatrix} e_1 = \tilde{y}_1 = z_1 - z_{1_d} \\ e_2 = \tilde{y}_2 = z_2 - z_{2_d} \\ e_3 = \tilde{y}_3 = z_3 - z_{3_d} \end{Bmatrix} \tag{61}$$

$$\begin{Bmatrix} \dot{e}_4 = \dot{\tilde{y}}_4 = \dot{z}_4 - \dot{z}_{4_d} \\ \dot{e}_5 = \dot{\tilde{y}}_5 = \dot{z}_5 - \dot{z}_{5_d} \\ \dot{e}_6 = \dot{\tilde{y}}_6 = \dot{z}_6 - \dot{z}_{6_d} \end{Bmatrix} \tag{62}$$

Where $z = \begin{bmatrix} e_1 & e_2 & e_3 & e_4 & e_5 & e_6 \end{bmatrix}^T$ or $z = \begin{bmatrix} e & \dot{e} \end{bmatrix}^T$ is represented as the new state variable and the linearized model after feedback linearization is yielded.

From Eq. (27) , $u = E(u_c + \bar{u})$ and it is included faults into the actuators. By considering following equations,

10.22060/EEJ.2026.25440.5933

$$\dot{z} = Az + Bv \tag{63}$$

$$y = Cz \tag{64}$$

Eq. (65) is represented the continuous-time space equations.

$$A = \begin{bmatrix} 0_3 & I_3 \\ 0_3 & 0_3 \end{bmatrix}, B = \begin{bmatrix} 0_3 \\ I_3 \end{bmatrix}, C = \begin{bmatrix} I_3 & 0_3 \end{bmatrix} \tag{65}$$

Eq. (66) is discretized the Eq. (63).

$$z(k+1) = A_d z(k) + B_d v \tag{66}$$

$$A_d = I_3 + t_s A, B_d = t_s B \tag{67}$$

The related control law is signified as follows and the virtual control input was introduced in Eq.(51),So in order to considering actuator faults and external disturbance into the closed loop stability analysis, the Eq.(27) is substituted into the Eq.(68) and Eq. (69) is yielded.

$$\ddot{y} = E(x(k)) + D(x(k))u \tag{68}$$

$$v = E(x(k)) + D(x(k))(u + d_{disturbance}) \tag{69}$$

by considering $z = \begin{bmatrix} e & \dot{e} \end{bmatrix}^T$ and P as a symmetric positive definitive matrix the above equations are derived rigorously.

By choosing candidate Lyapunov function in Eq. (70) and Eq. (71) is the linear feedback controller of the system.

$$V = z^T P z \tag{70}$$

10.22060/EEJ.2026.25440.5933

$$\boldsymbol{u} = -\boldsymbol{Kz} \tag{71}$$

Eq.(72) is outlined the control gain $\boldsymbol{K}$ and matrix $\boldsymbol{P}$ can be obtained by solving the Riccati algebraic Eq. (73).

$$\boldsymbol{K} = \boldsymbol{R}^{-1}\boldsymbol{B}^{T}\boldsymbol{P} \tag{72}$$

$$\boldsymbol{H}^{T}\boldsymbol{P} + \boldsymbol{PH} + \boldsymbol{Q} - \boldsymbol{PBR}^{-1}\boldsymbol{B}^{T}\boldsymbol{P} = 0 \tag{73}$$

and the symmetric positive definitive matrix $\boldsymbol{P}$ is able to find by holding the true Lyapunov function.

$$\boldsymbol{P}^{T}\boldsymbol{H} + \boldsymbol{HP} = -\boldsymbol{I} \tag{74}$$

Where

$$\boldsymbol{H} = \begin{bmatrix} 0 & 1 & 0 & 0 & 0 & 0 \\ 0 & 0 & 1 & 0 & 0 & 0 \\ 0 & 0 & 0 & 1 & 0 & 0 \\ 0 & 0 & 0 & 0 & 1 & 0 \\ 0 & 0 & 0 & 0 & 0 & 1 \\ -\boldsymbol{K}_1 & -\boldsymbol{K}_2 & -\boldsymbol{K}_3 & -\boldsymbol{K}_4 & -\boldsymbol{K}_5 & -\boldsymbol{K}_6 \end{bmatrix} \tag{75}$$

$$\boldsymbol{K}_{e} = \begin{bmatrix} \boldsymbol{K}_1 \\ \boldsymbol{K}_2 \\ \boldsymbol{K}_3 \end{bmatrix}, \boldsymbol{K}_{\dot{e}} = \begin{bmatrix} \boldsymbol{K}_4 \\ \boldsymbol{K}_5 \\ \boldsymbol{K}_6 \end{bmatrix} \tag{76}$$

10.22060/EEJ.2026.25440.5933

$$\dot{V} = z^T P z + z^T P \dot{z} = -z^T z + 2z^T \begin{bmatrix} 1 & 0 & 0 & 0 & 0 & 0 \end{bmatrix}^T D(x(k))(u + d_{disturbance}) = \\ -z^T z + 2\dot{y}^T (D(x(k))(u + d_{disturbance})) \tag{77}$$

So $V \succ 0$ and $\dot{V} \leq 0$ and the system is asymptotically stable.

5-Benchmark Results

In this section, we will investigate the feasibility and performance of the proposed hybrid controller. The simulations are conducted under arbitrary numerical conditions. for this section the information of this flexible satellite is chosen from[31]. All figures are categorized into two different states, and the performance of the hybrid controller is analyzed after a fault occurs in the actuators. One drawback of Model Predictive Control (MPC) is its poor performance when dealing with low-frequency vibration ranges and the combination of Lyapunov Nonlinear Model Predictive Control (LNMPC) and Feedback Linearization (FBL) effectively addresses the problem. Furthermore, in all plots, 30 percent of the satellite's moment of inertia is considered as uncertainty. Tables 1 to 3 present the system parameters used in the simulations. The remaining coefficient values are $K_e = diag([1,1,1])$ and $K_{\dot{e}} = diag([7,7,7])$. $R = diag([10,10,10])$ and $Q = diag([1500,1500,1500,1500,1500,1500])$ and the vibration frequencies of the appendages are $\Omega_f = diag([0.76811,1.1038,1.8733])$ also specified. The diagonal matrix $E = diag([0.6, 0.5, 0.4])$ is the actuators loss of effectiveness. The external torque disturbance that is employed to the actuators, is based [32]. It is assumed that flexible satellite is maneuvering in an orbit with attitude of 500 Km from the earth surface, and the total torque disturbance is considered as follows,

$$d_{disturbance} = 2 \times \begin{bmatrix} \cos(\omega_0 t) + 1 \\ \cos(\omega_0 t) + \sin(\omega_0 t) \\ \sin(\omega_0 t) + 1 \end{bmatrix} \tag{78}$$

To analysis the robustness of the proposed controller, the domain of the disturbance is increased to 2 and the orbital angular velocity (ω_0) is 0.0011rad/s. Table 1 introduces the system parameters. the parameters related to actuators are $R_\alpha = 1$, $K_b = 0.0005$, $K_m = 0.2$, $b = (1.21) \times 10^{-3}$ and reaction wheels momentum of inertia is

$$I_\omega = \begin{bmatrix} 10 & 0 & 0 \\ 0 & 10 & 0 \\ 0 & 0 & 10 \end{bmatrix} \tag{79}$$

10.22060/EEJ.2026.25440.5933

Table 1. System parameters

Number	Parameter	Value
1	$\boldsymbol{\delta}$	$\begin{bmatrix} 6.45637 & 1.27814 & 2.15629 \\ -1.25819 & 0.91756 & -1.67264 \\ 1.11687 & 2.48901 & -0.83674 \end{bmatrix}$
2	$\boldsymbol{\delta}_p$	$\begin{bmatrix} 70.26 & -4.23 & 2.34 \\ 4.80 & 31.96 & 1.24 \\ -1.05 & 2.55 & 29.84 \end{bmatrix}$
3	$\boldsymbol{P}$	$\begin{bmatrix} 0.3 & 0 & 0 \\ 0 & 0.3 & 0 \\ 0 & 0 & 0.3 \end{bmatrix}$
4	$\boldsymbol{I}_s$	$\begin{bmatrix} 350 & 3 & 4 \\ 3 & 270 & 10 \\ 4 & 10 & 190 \end{bmatrix}$

5-1-Simulation Results

Figs. 4 to 10 illustrate the results of the simulations. Fig. 4 shows the satellite's Euler angles after introducing faults into the reaction wheels; despite experiencing a significant overshoot, the angles ultimately reached their desired attitude. Fig. 5 displays the control effort signals from the actuators. Even in the presence of faults, uncertainties, and a significant torque disturbance, the control efforts were sufficient to address these challenges.

Figs. 6 and 8 demonstrate that the flexible appendage's vibration displacements and Piezoelectric voltage input respectively, which is a key objective of this study, in order to prevent satellite stability to be interrupted it is necessary to neutralize the satellite vibration. Fig. 7 illustrates Flexible satellite angular momentum, Fig. 9 depicts Modified Rodriguez Parameters.

Fig. 10 pertains to the Reaction wheels motors angular velocities. and it is indicated that the hybrid controller could properly stop reaction wheels after maneuvering. and this is one of the tasks that the proposed controller should handle it.

According to the figures, the Euler angles settling times has been a little longer after the employing fault to the actuators and this event is completely normal due to actuators loss of effectiveness. So in the subsection

AUT Journal of Electrical Engineering
10.22060/EEJ.2026.25440.5933

5.2 the Cascade ESO is utilized to improve hybrid controller performance in the presence of actuators fault, external disturbance and uncertainty.

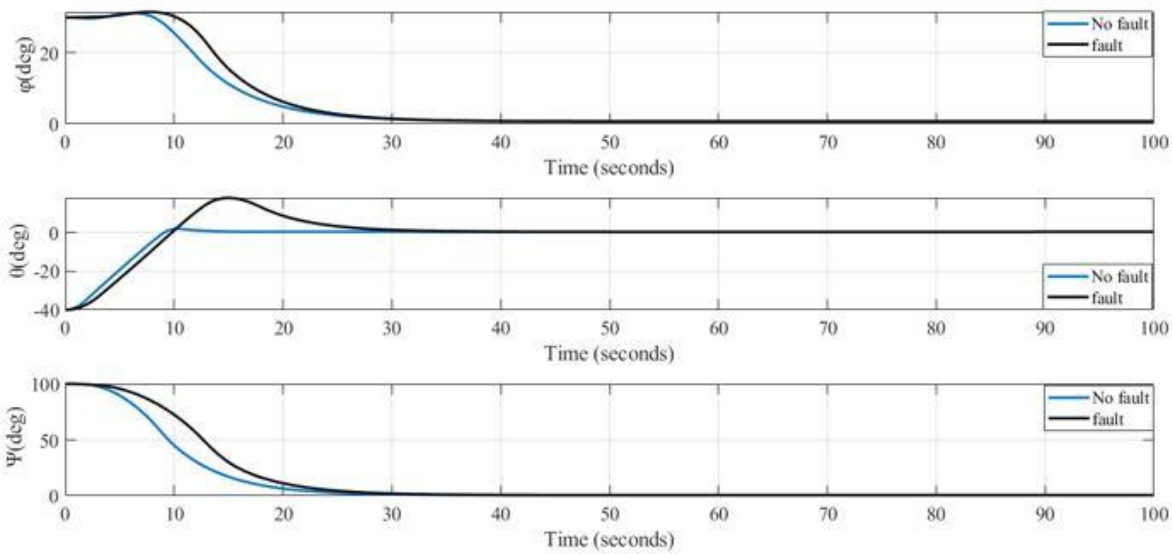

Fig.4.Flexible satellite euler angles

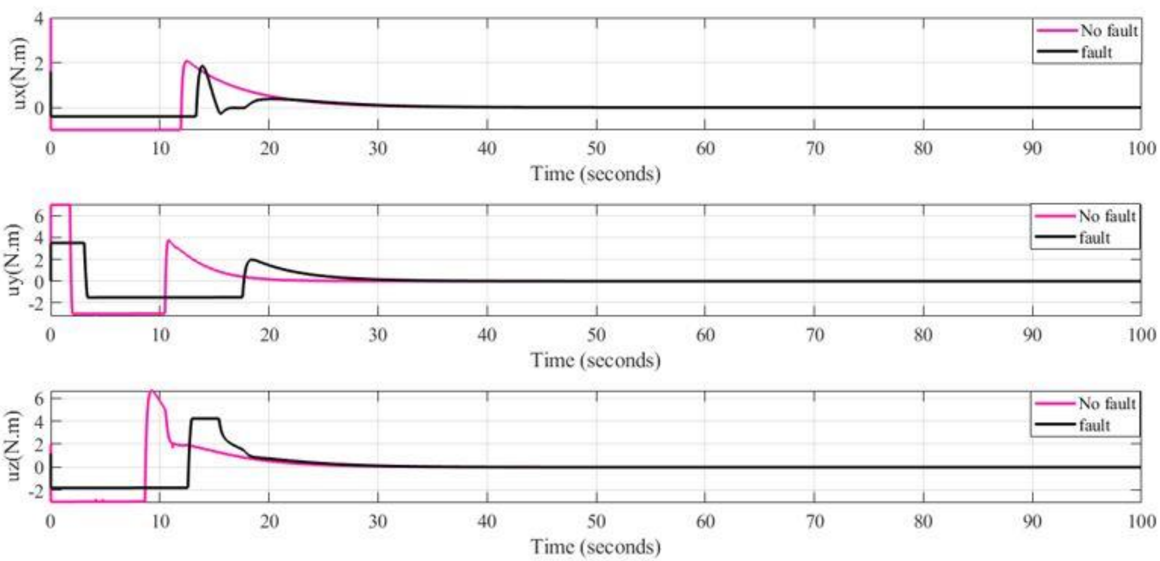

10.22060/EEJ.2026.25440.5933

Fig.5.Control Effort Signals

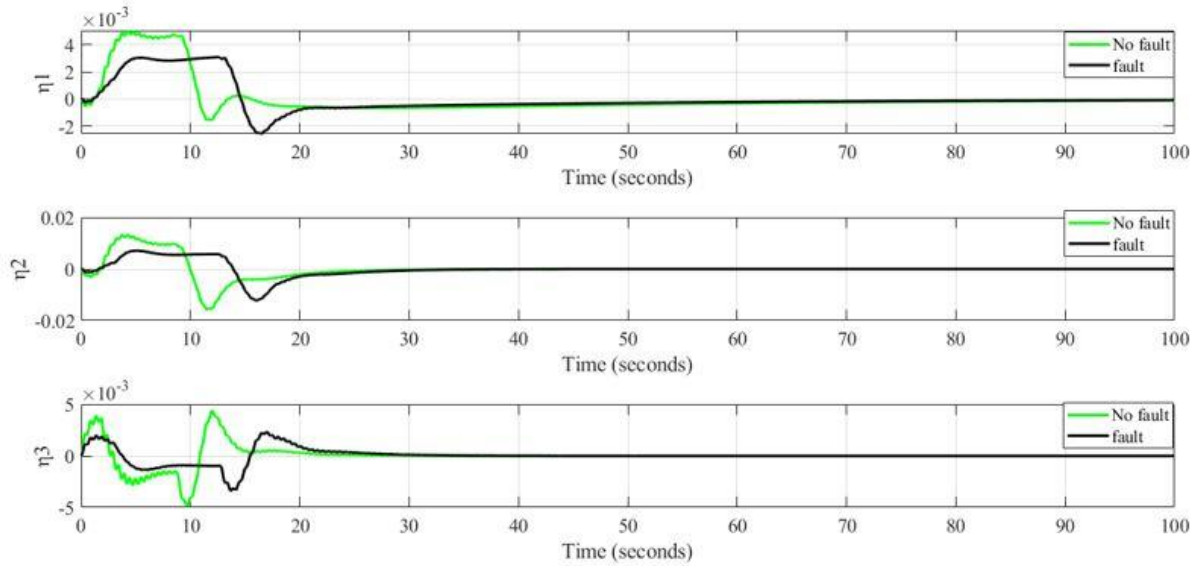

Fig.6.Flexible satellite's vibration displacements

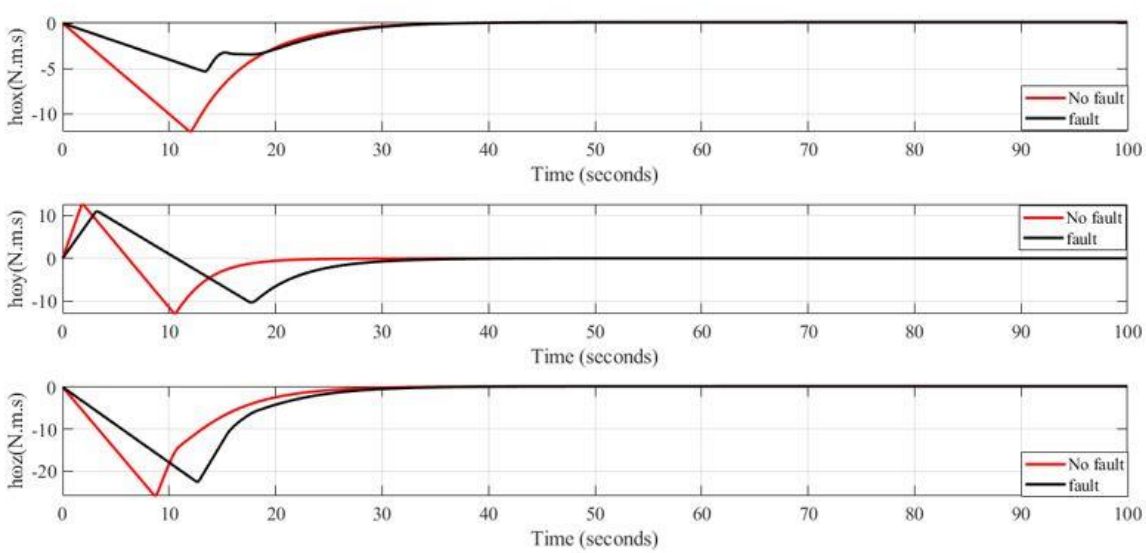

Fig.7.Flexible satellite angular momentum

AUT Journal of Electrical Engineering
10.22060/EEJ.2026.25440.5933

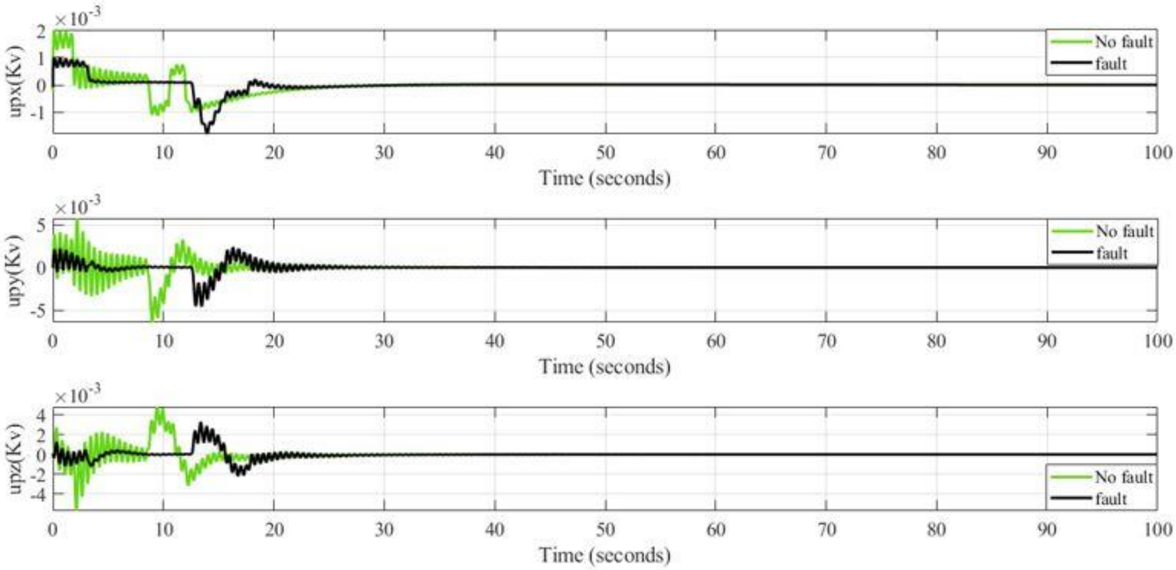

Fig.8.piezoelectric actuators voltage input

10.22060/EEJ.2026.25440.5933

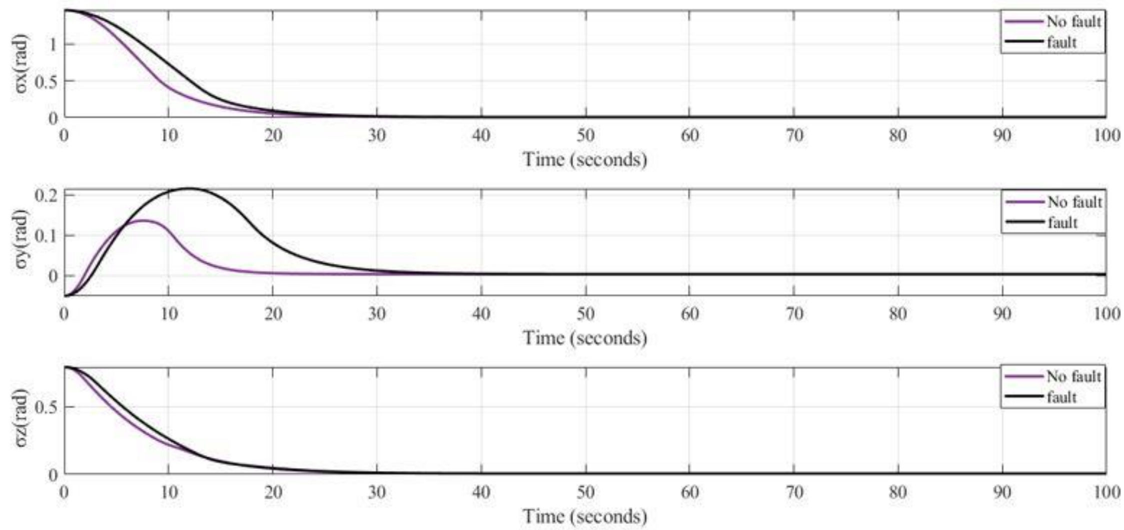

Fig.9. Rodriguez parameters

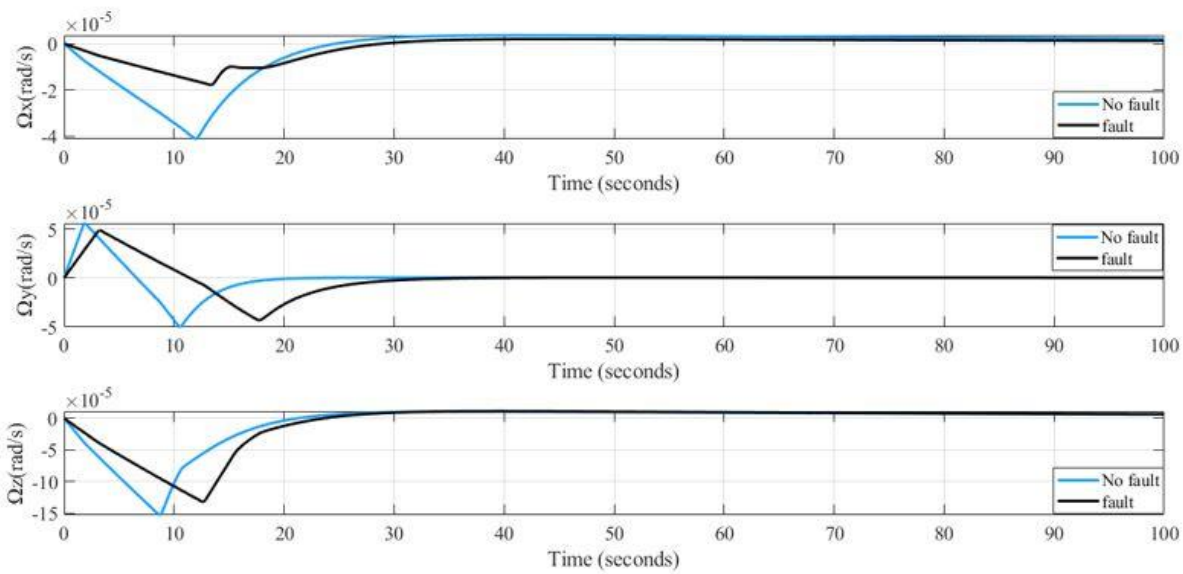

Fig.10. Reaction wheels motors angular velocities

10.22060/EEJ.2026.25440.5933

Table2. Hybrid controller specifications during actuator faults

Method name	Euler angles settling time(s)	Max torque(N. m)	Vibrations displacement	Settling time(s)
No fault	$\phi = 28$		$\eta_1 = 0.045$	$\eta_1 = 20$
	$\theta = 10$	5	$\eta_2 = 0.015$	$\eta_2 = 20.7$
	$\psi = 25$		$\eta_3 = 0.003$	$\eta_3 = 22$
fault	$\phi = 38$	5	$\eta_1 = 0.025$	$\eta_1 = 22$
	$\theta = 30$		$\eta_2 = 0.01$	$\eta_2 = 21$
	$\psi = 29$		$\eta_3 = 0.002$	$\eta_3 = 25$

5-2-Cascade ESO simulation results

In this subsection, the performance of the Cascade ESO is investigated. Fig. 11 depicts the control efforts and Fig. 12 is about Euler angles. Figs. 13 and 14 are flexible appendage's vibration displacements and angular momentum respectively .Fig.15 is Piezoelectric voltage input . the tuned parameters are, $\beta_1 = 10, \beta_2 = 50, \beta_3 = 50, \beta_4 = 50, \alpha_1 = 0.1, \alpha_2 = 0.1, \bar{b}_0 = 0.001, \delta_1 = 0.1, \delta_2 = 0.1$.

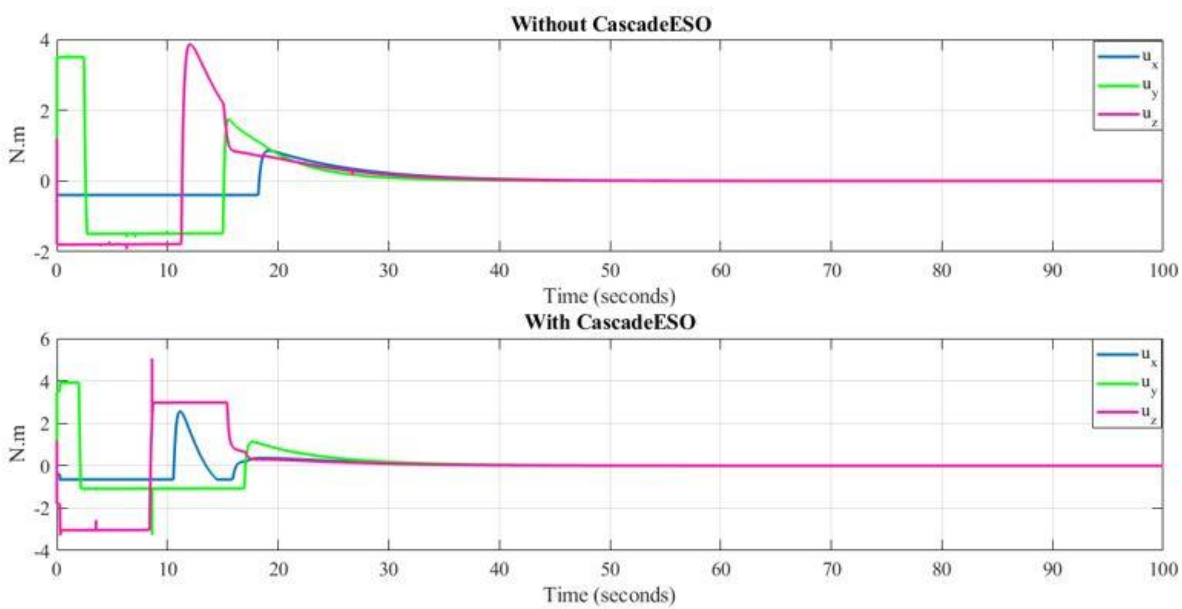

Fig.11. Control effort signals

AUT Journal of Electrical Engineering
10.22060/EEJ.2026.25440.5933

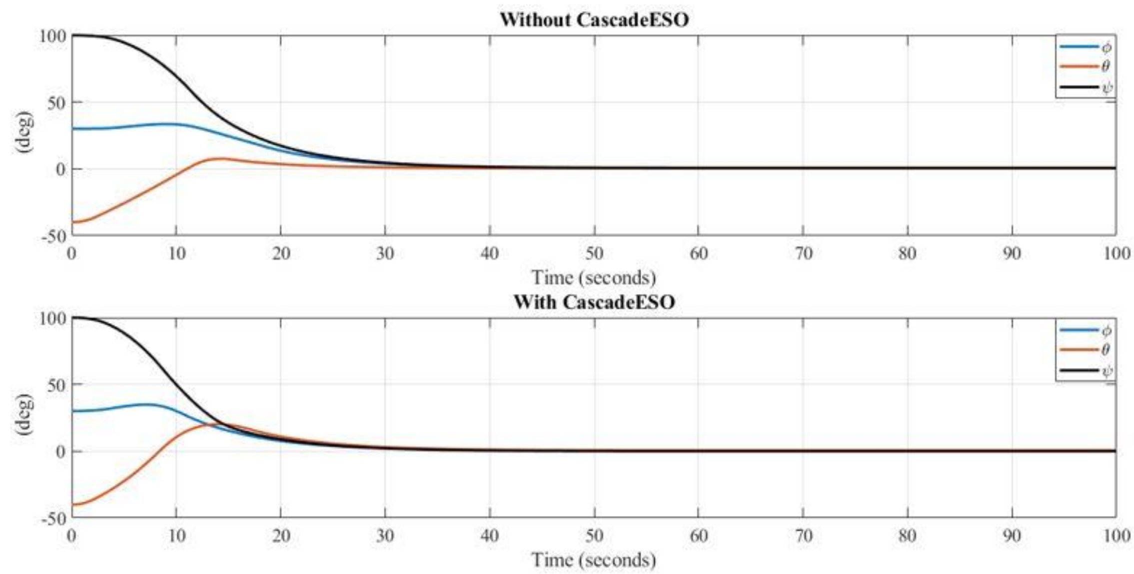

Fig.12.flexible satellite Euler angles

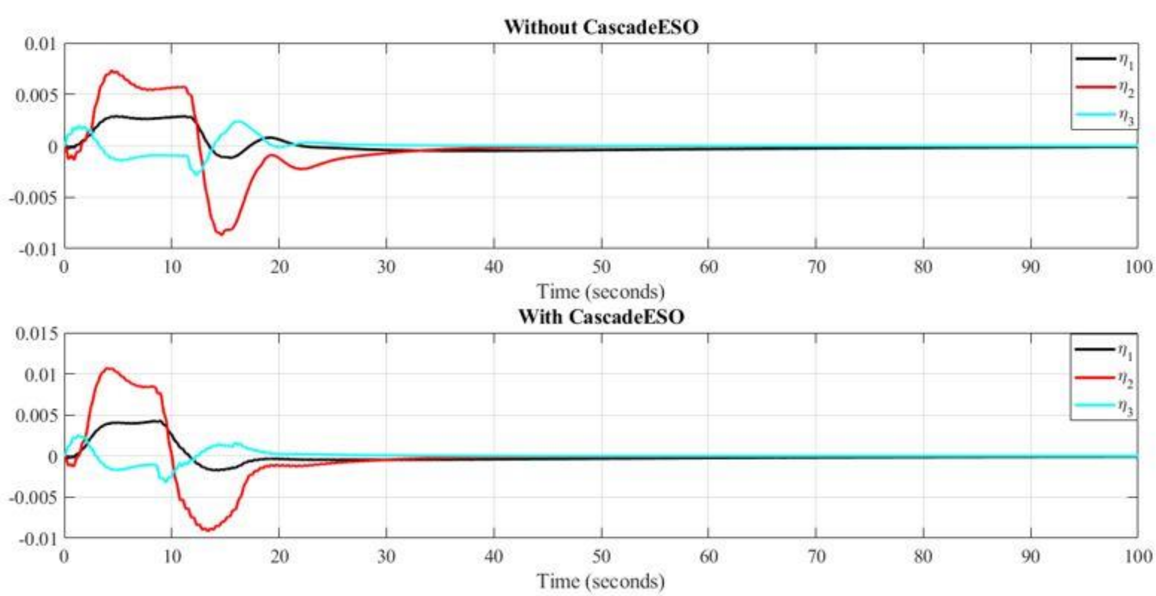

Fig.13.Flexible appendage’s vibration displacements

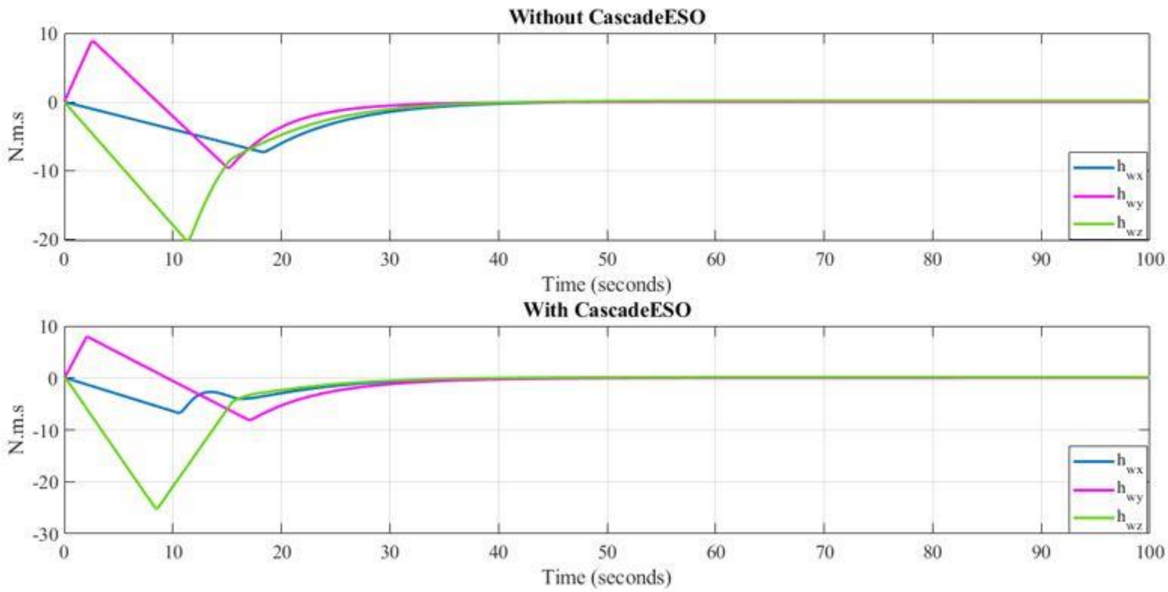

Fig.14. Flexible satellite angular momentums

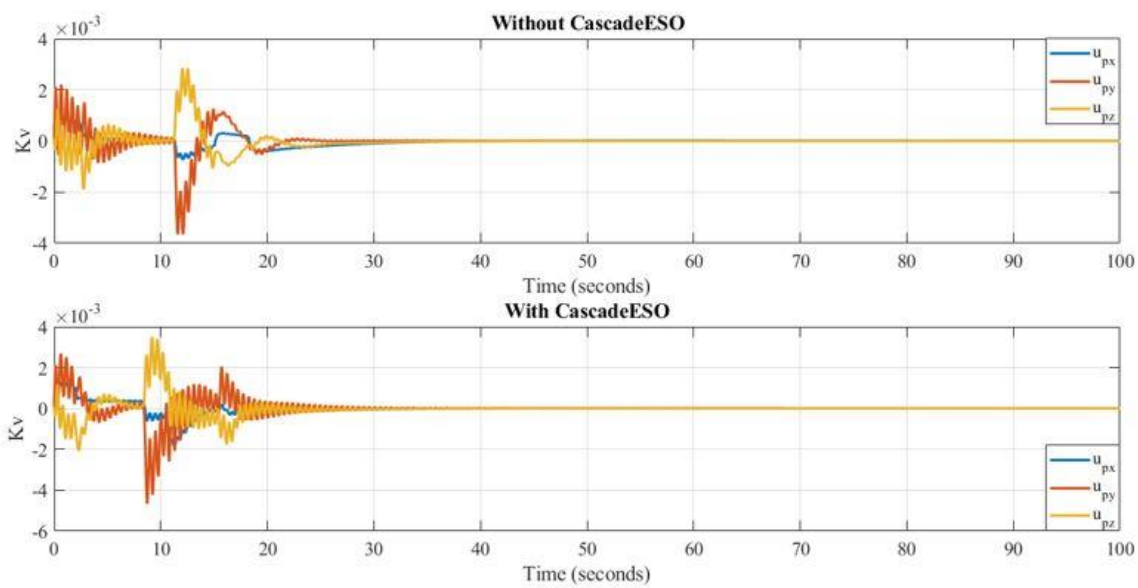

10.22060/EEJ.2026.25440.5933

Fig.15. Piezoelectric voltage inputs

Table3. Comparison of controller performance with and without Cascade ESO

Method	Euler angles settling time(s)	Max torque(N. m)	Vibration displacements	Vibration settling time(s)
Without Cascade ESO	$\phi = 35$ $\theta = 35$ $\psi = 35$	5	$\eta_1 = 0.001$ $\eta_2 = 0.004$ $\eta_3 = 0.005$	$\eta_1 = 32$ $\eta_2 = 31$ $\eta_3 = 30$
With Cascade ESO	$\phi = 28$ $\theta = 28$ $\psi = 28$	5	$\eta_1 = 0.004$ $\eta_2 = 0.01$ $\eta_3 = 0.003$	$\eta_1 = 22$ $\eta_2 = 21$ $\eta_3 = 20$

5-3-Fact Checking

For paper fact checking this Ref[17] is utilized. The comparison between two methods are put in the below diagrams.

$$\boldsymbol{J}_{ref\,[17]} = \begin{bmatrix} 487 & 15 & -1.2 \\ 14.9 & 177 & -7.3 \\ -1.2 & -7.3 & 404 \end{bmatrix} \quad \textbf{(79)}$$

$$\boldsymbol{\delta}_{ref\,[17]} = \begin{bmatrix} 1 & 0.1 & 0.1 \\ 0.5 & 0.1 & 0.01 \\ -1 & 0.3 & 0.01 \end{bmatrix} \quad \textbf{(80)}$$

Eqs. (79) and (80) are flexible satellite momentum of inertia and coupling matrix related to the Ref[17] respectively. Fig. 16 is the Euler angles comparison, Fig. 17 is the control effort comparison, Fig. 18 is the flexible appendage's vibration displacements comparison, Figs. 19 and 20 are flexible satellite angular

10.22060/EEJ.2026.25440.5933

momentums and piezoelectric voltage respectively, and Figs. 21 and 22 are Modified Rodriguez Parameters and reaction wheels motors angular velocities comparison respectively.

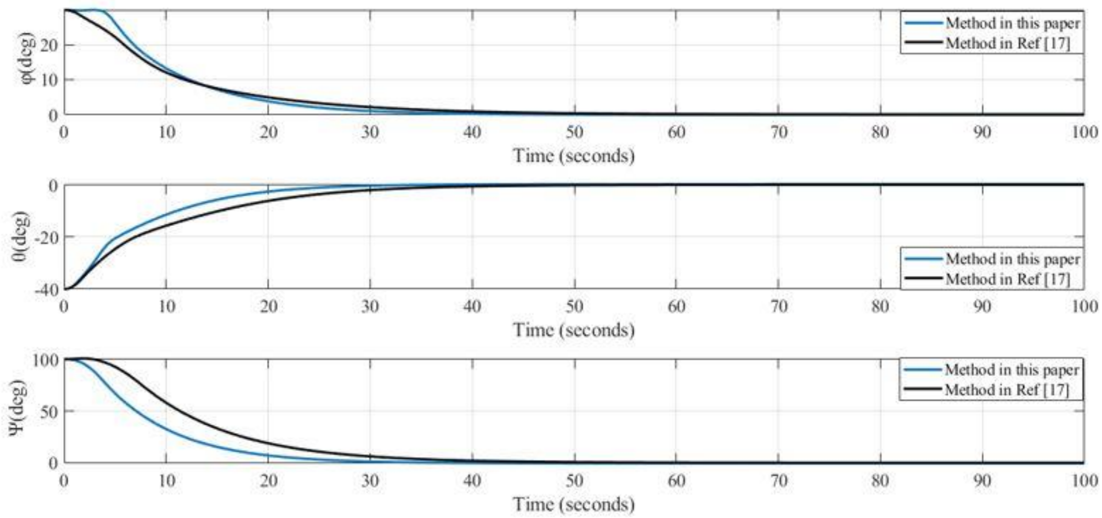

Fig.16.Flexible satellite Euler angles comparison

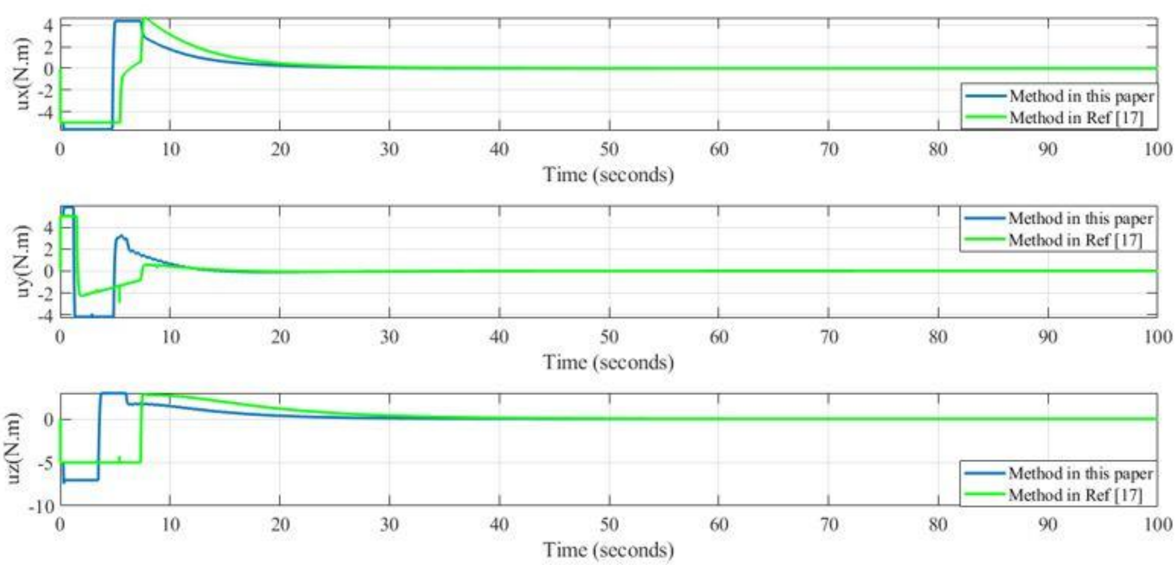

Fig.17.Control effort signals comparison

AUT Journal of Electrical Engineering
10.22060/EEJ.2026.25440.5933

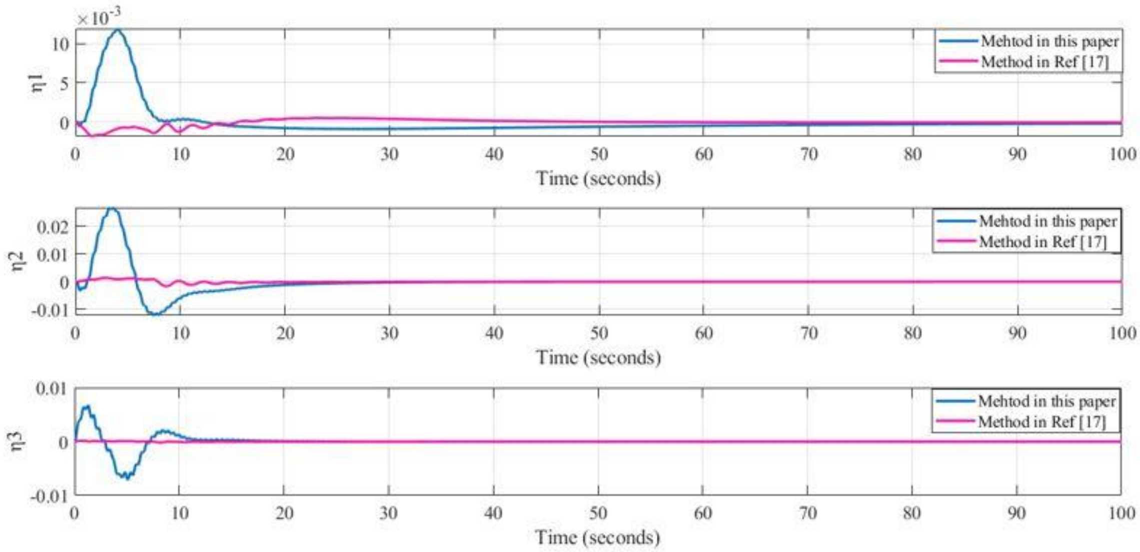

Fig.18.Flexible appendage's vibration displacements comparison

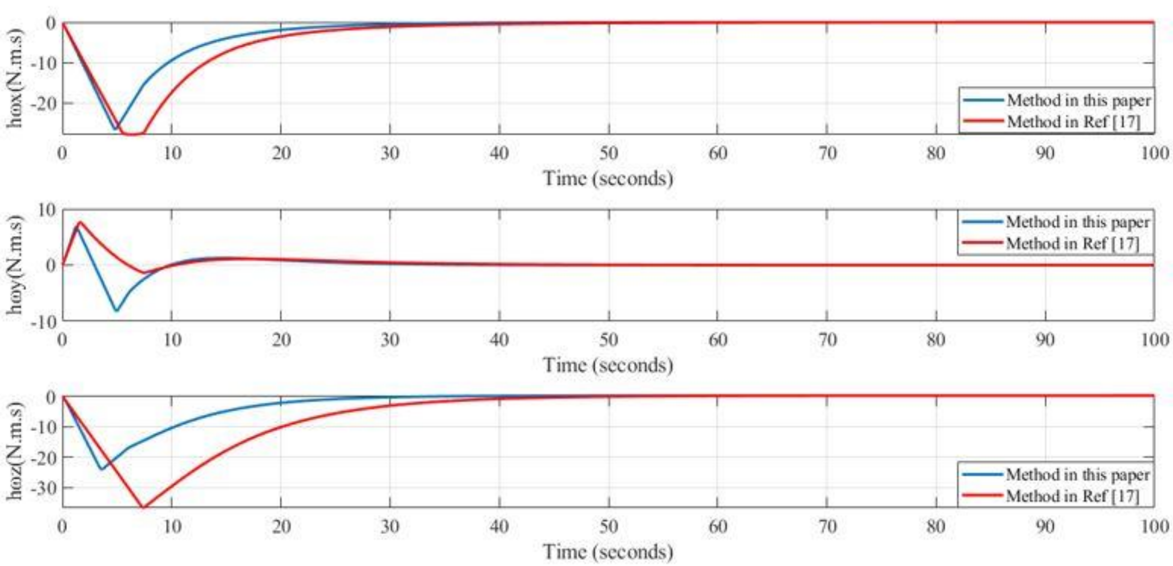

Fig.19.Flexible satellite angular momentums comparison

10.22060/EEJ.2026.25440.5933

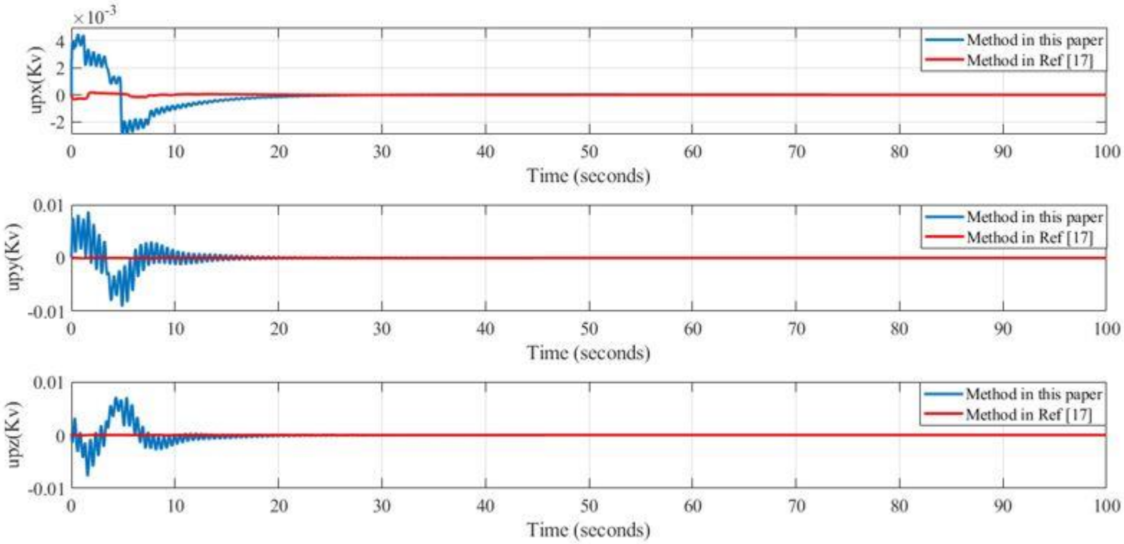

Fig.20.Piezoelectric voltage inputs comparison

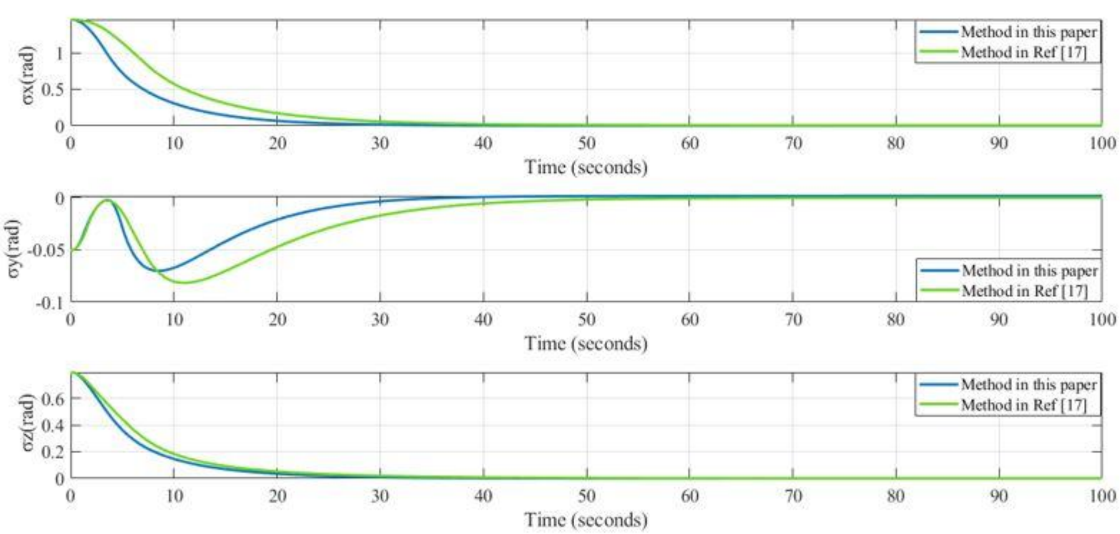

Fig.21.Flexible satellite modified Rodriguez parameters(MRPs)comparison

10.22060/EEJ.2026.25440.5933

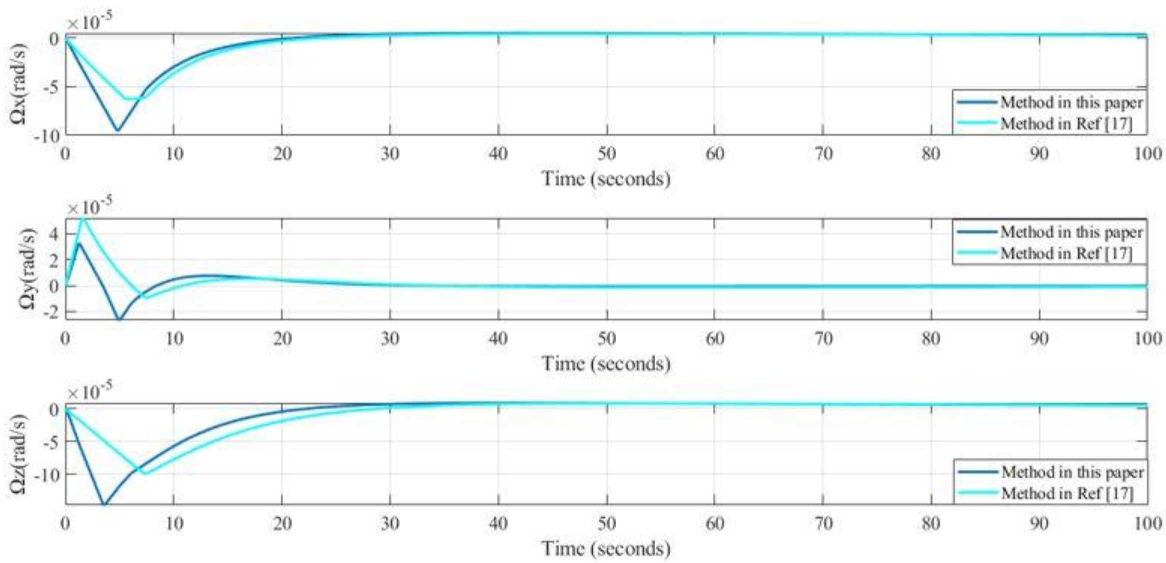

Fig.22.Flexible satellite reaction wheels motors angular velocities comparison

Table 4. Two methods comparison

Method name	Euler angles settling time(s)	Max torque(N. m)	Vibration Displacements	Vibration Displacements settling time(s)
Method in this paper	$\phi = 28$ $\theta = 30$ $\psi = 29$	5	$\eta_1 = 0.006$ $\eta_2 = 0.002$ $\eta_3 = 0.001$	$\eta_1 = 12$ $\eta_2 = 20$ $\eta_3 = 11$
Method in ref[17]	$\phi = 35$ $\theta = 35$ $\psi = 38$	5	$\eta_1 = 0.0001$ $\eta_2 = 0.0001$ $\eta_3 = 0.00001$	$\eta_1 = 5$ $\eta_2 = 15$ $\eta_3 = 1$

According to the Table 4, the Euler angles in hybrid controller in this paper have shorter settling times and also vibration displacements have lower values rather than method in Ref[17], so it is obtained from that table that the hybrid controller in this paper has improved the flexible satellite stability as well. This algorithm has properly enhance the effect of the performance of the system.

6-conclusion

This paper explores a composite controller designed for the attitude control of flexible satellite. The objective of the controller is to reduce the angular velocities of both the satellite and the reaction wheels to zero following each maneuver. The study evaluates the performance of this composite controller under various conditions, including uncertainties, actuator faults, and torque disturbances. The Feedback Linearization (FBL) method is a category of nonlinear control strategies that achieves high accuracy by canceling out the nonlinearity in system dynamics. It effectively eliminates vibrations in flexible satellites. By integrating FBL with Lyapunov Nonlinear Model Predictive Control (LNMPC), the resulting hybrid controller exhibits robustness and the ability to withstand various uncertainties, actuator faults, and disturbances. LNMPC is a robust family of Model Predictive Control (MPC) methods capable of handling significant external disturbances and uncertainties. Merging FBL with LNMPC was a suitable choice given that the vibration frequency of flexible satellites often falls within a low range. In such cases, LNMPC alone may not effectively dampen vibrations, making FBL essential for vibration reduction. FBL serves as a nonlinear controller that linearizes the input/output relationship of the system. Additionally, it reduces computational burden and enhances tracking accuracy. For future works this hybrid algorithm can be used in flexible satellite formations for instance leader-follower method and it would assist to enhance the follower satellite performance in the presence of the leader faults or failures. further more, implementation of the proposed algorithm on a satellite simulator will be completely possible in real time.

References

[1] S. Ahmed and E. C. Kerrigan, ``Suboptimal Predictive Control for Satellite Detumbling, Journal of Guidance, Control, and Dynamics, vol. 37, no. 3, pp. 850-859, 2014, doi: 10.2514/1.61367.

[2] W.-H. C. Yi Cao, ``Automatic Differentiation based Nonlinear Model Predictive Control of Satellites using Magneto-Torquers, IEEE, 2009.

[3] K. Kondo, I. Kolmanovsky, Y. Yoshimura, M. Bando, S. Nagasaki, and T. Hanada, ``Nonlinear Model Predictive Detumbling of Small Satellites with a Single-Axis Magnetorquer, Journal of Guidance, Control, and Dynamics, vol. 44, no. 6, pp. 1211-1218, 2021, doi: 10.2514/1.G005877.

[4] J. A. Starek and I. V. Kolmanovsky, ``Nonlinear model predictive control strategy for low thrust spacecraft missions, Optimal Control Applications and Methods, vol. 35, no. 1, pp. 1-20, 2012, doi: 10.1002/oca.2049.

[5] T. Rybus, K. Seweryn, and J. Z. Sasiadek, Control System for Free-Floating Space Manipulator Based on Nonlinear Model Predictive Control (NMPC), Journal of Intelligent \& Robotic Systems, vol. 85, no. 3-4, pp. 491-509, 2016, doi: 10.1007/s10846-016-0396-2.

[6] A. Alouache, ``Nonlinear Model Predictive Control for Trajectory Tracking and Obstacle Avoidance of Free-Floating Satellite Manipulator, Journal of Advanced Engineering and Computation, vol. 8, no. 2, 2024, doi: 10.55579/jaec.202482.455

[7] L. A. M. Wei Wang, Shinkyu Park, Pietro Leoni, Banti Gheneti, and C. R. a. D. R. Fabio Duarte, Design, Modeling, and Nonlinear Model Predictive Tracking Control of a Novel Autonomous Surface Vehicle, IEEE, 2018.

[8] Y. Wang, M. Soltani, and D. M. A. Hussain, ``Attitude stabilization of Marine Satellite Tracking Antenna using Model Predictive Control, IFAC Journal of Systems and Control, vol. 17, 2021, doi: 10.1016/j.ifacsc.2021.100173.

[9] K. V. L. Xiaohua Zhang, Zhengliang Lu, Xiang Zhang, Wenhe Liao, W.S. Lim, ``Piece-wise affine MPC-based attitude control for a CubeSat during orbital manoeuvres, Elsevier, Aerospace Science and Technology, 2021, doi: 10.1016/j.ast.2021.106997.

[10] S. Kalaycioglu and A. de Ruiter, ``Vibration Control of Satellite Antennas via NMPC and NARX Neural Networks,IEEE Transactions on Aerospace and Electronic Systems,pp. 1-29, 2025, doi: 10.1109/taes.2025.3551276.

[11] M. AlandiHallaj and N. Assadian, Multiple-horizon multiple-model predictive control of electromagnetic tethered satellite system, Acta Astronautica , vol. 157, pp. 250-262, 2019, doi: 10.1016/j.actaastro.2018.11.003.

[12] M. Khodaverdian and M. Malekzadeh, ``Attitude stabilization of spacecraft simulator based on modified constrained feedback linearization model predictive control, IET Control Theory \& Applications, vol. 17, no. 8, pp. 953-967, 2023, doi: 10.1049/cth2.12429.

[13] Z. Cai, S. Zhang, and X. Jing, Model Predictive Controller for Quadcopter Trajectory Tracking Based on Feedback Linearization, IEEE Access, vol. 9, pp. 162909-162918, 2021, doi: 10.1109/access.2021.3134009.

[14] Y. Z. Mohamed A. Kamel, ``Linear Model Predictive Control via Feedback Linearization for Formation Control of Multiple Wheeled Mobile Robots, IEEE International Conference on Information and Automation, Lijiang, China, August 2015, 2015.

[15] P. E. Fabian Schnelle, Constraint mapping in a feedback linearization/MPC scheme for trajectory tracking of underactuated multibody systems, Elsevier, 2015.

[16]J. A. M. Jack Caldwell, ``Towards Efficient Learning-Based Model Predictive Control via Feedback Linearization and Gaussian Process Regression, IEEE, 2021.

[17] M. M. Maria Khodaverdian, ``Fault-tolerant model predictive sliding mode control with fixed-time attitude stabilization and vibration suppression of flexible spacecraft, Elsevier, Aerospace Science and Technology, 2023, doi: 10.1016/j.ast.2023.108381.

[18] Wenmen You, Xiangpeng Xie, Hui Wang , Jianwei Xia ,Vladimir Stojanovic, Relaxed Model Predictive Control of T-S Fuzzy Systems via a New Switching-Type Homogeneous Polynomial Technique, IEEE Transactions of Fuzzy Systems, 2024,doi: 10.1109/TFUZZ.2024.3405078

[19]Marcelo Menezes Morato , Emanuel Bernardi , Vladimir Stojanovich , A qLPV Nonlinear Model Predicitve Control with Moving Horizon Estimation , Complex Engineering Systems , 2021 , doi: 10.20517/ces.2021.09

[20] Morteza Salehipour, Maryam Malekzadeh, Mahdi Mortazavi, Mohammad Sayanjali, AUT Journal of Mechanical Engineering,2025,doi: 10.22060/ajme.2025.24218.6184

[21] T.P. Sales , D.A. Rade, L.C.G. de Souza , Passive vibration control of flexible spacecraft using shunted piezoelectric transducers, Aerospace Science and Technology , 2013 , doi: 10.1016/j.ast.2013.05.001

[22] M. Azadi, M. Eghtesad, S.A. Fazelzadeh, E. Azadi, Dynamics and control of a smart flexible satellite moving an orbit, Springer, doi: 10.1007/s11044-014-9447-2

[23] S. M. SYED MUHAMMAD AMRR, IEEE), MASHUQ UN NABI, (Member, IEEE), An Event-Triggered Robust Attitude Control of Flexible Spacecraft With Modified Rodrigues Parameters Under Limited Communication, IEEE, 2019, doi: 10.1109/ACCESS.2019.2927616.

[24] Q. Hu, ``Sliding mode maneuvering control and active vibration damping of three-axis stabilized flexible spacecraft with actuator dynamics, Springer, 2008, doi: 10.1007/s11071-007-9274-6.

[25] S. Zhu, D. Wang, Q. Shen, and E. K. Poh, Satellite Attitude Stabilization Control with Actuator Faults, Journal of Guidance, Control, and Dynamics, vol. 40, no. 5, pp. 1304-1313, 2017, doi: 10.2514/1.G001922.

[26]D. J. P. a. G.A. Andrade a, J.D. A´ lvarez c, M. Berenguel ``A practical NMPC with robustness of stability applied to distributed solar power plants, Elsevier, 2013, doi: 10.1016/j.solener.2013.02.013.

[27] M. R. H. M. Navabi, Spacecraft Quaternion Based Attitude Input-Output Feedback Linearization Control Using Reaction Wheels, IEEE, 2017.

[28] W. R. van Soest, Q. P. Chu, and J. A. Mulder, ``Combined Feedback Linearization and Constrained Model Predictive Control for Entry Flight, Journal of Guidance, Control, and Dynamics, vol. 29, no. 2, pp. 427-434, 2006, doi: 10.2514/1.14511

[29]Liuping Wang, Model Predictive Control System Design and Implementation Using MATLAB, Springer-Verlag London Limited,2009,doi: 10.1007/978-1-84882-331-0

[30] S. D. Zhidan Yan, Zhenyu Yang, Xudong Zhao, Nan Yang, Yunfeng Lu ``Improved nonlinear active disturbance rejection control for a continuous-wave pulse generator with cascaded extended state observer, Elsevier, Control Engineering Practice, p. 15, 2024, doi: 10.1016/j.conengprac.2024.105897.

10.22060/EEJ.2026.25440.5933

[31] J. S. Ti Chen ``Rotation-Matrix-Based Attitude Tracking for Multiple Flexible Spacecraft with Actuator Faults, AIAA Guidance, Navigation, and Control Conference, p. 8, 2018, doi: 10.2514/1.G003812.

[32] C. Zhang, G. Ma, Y. Sun, and C. Li, ``Prescribed performance adaptive attitude tracking control for flexible spacecraft with active vibration suppression, Nonlinear Dynamics, vol. 96, no. 3, pp. 1909-1926, 2019, doi: 10.1007/s11071-019-04894-x.